NASA CR-135226

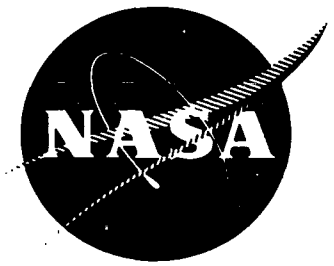

INERT GAS THRUSTERS

PREPARED FOR

LEWIS RESEARCH CENTER

NATIONAL AERONAUTICS AND SPACE ADMINISTRATION

GRANT NSG 3011

Annual Report

July 1977

Harold R. Kaufman

Department of Mechanical Engineering
Colorado State University
Fort Collins, Colorado

1. Report No.	2. Government Accession No.	3. Recipient's Catalog No.
CR-135226		

4. Title and Subtitle	5. Report Date
INERT GAS THRUSTERS (U)	July 1977
	6. Performing Organization Code
7. Author(s)	8. Performing Organization Report No.
Harold R. Kaufman	
	10. Work Unit No.
9. Performing Organization Name and Address	11. Contract or Grant No.
Department of Mechanical Engineering Colorado State University Fort Collins, Colorado 80523	NSG 3011
	13. Type of Report and Period Covered
12. Sponsoring Agency Name and Address	Contractor report 1 Aug. 1976 - 30 July 1977
National Aeronautics and Space Administration Washington, D.C. 20546	14. Sponsoring Agency Code

15. Supplementary Notes

Grant Manager, Vincent K. Rawlin
NASA Lewis Research Center
Cleveland, Ohio 44135

16. Abstract

Inert gases, particularly argon and xenon, are of interest as possible alternatives to the usual electric thruster propellants of mercury and cesium. Advances in discharge-chamber technology have been covered in a separate publication (NASA CR-135101). Hollow cathode data were obtained for a wide range of operating conditions. Some test conditions gave plasma coupling voltages at or below the sputtering threshold, hence should permit long operating lifetimes. All observations of hollow cathode operation were consistent with a single theory of operation, in which a significant amount of the total electron emission is from localized areas within the orifice. This mode of emission is also supported by scanning electron microscope photographs that indicate local temperatures at or near the melting temperature of the tungsten tip. Experimental hollow cathode performance was correlated for two orifice diameters, three inert gas propellants, and a range of flow rates for each propellant. The degree of correlation obtained was excellent considering the preliminary nature of this correlation study. The basic theory for the production of doubly ionized argon and xenon has been completed. Experimental measurements of the doubly ionized fraction agree with theory within about ±20 percent. High voltage isolators were studied for the propellant feed line. The breakdown voltage per segment ranged from 300 to over 500 V with argon.

17. Key Words (Suggested by Author(s))	18. Distribution Statement
Electric Propulsion Ion Beams Ion Sources	Unclassified-Unlimited

19. Security Classif. (of this report)	20. Security Classif. (of this page)	21. No. of Pages	22. Price*
Unclassified	Unclassified		

* For sale by the National Technical Information Service, Springfield, Virginia 22161

TABLE OF CONTENTS

LIST OF FIGURES

I - INTRODUCTION

The use of inert gases in electric thrusters was studied in this investigation. Of the inert gases, the one whose physical characteristics are most suited to space propulsion is xenon. High atomic weight and ease of storage with low tankage fraction are the major factors in this choice. Argon is a more economical alternative for space propulsion if a large amount of propellant is required (so that cryogenic storage is practical) and readily available electric power makes efficiency (and hence atomic weight) less important. Argon is also the preferred propellant for the sputter etching and deposition applications of thruster technology. Performance with argon is a larger departure from the usual thruster performance with mercury or cesium, hence argon was emphasized over xenon. Inert gases other than argon or xenon were also used to obtain better insight into various physical processes.

The major efforts of this investigation were on the discharge chamber, the hollow cathode, and the doubly charged ion model. There was a smaller effort on the isolator. The advances in discharge-chamber technology have been included in a recent publication on multipole gas thruster design[1] and will not be repeated here. The advances in the other areas are included herein, with a section devoted to each area. SI (rationalized mks) units are used in this report unless otherwise indicated.

II - HOLLOW CATHODE

by Larry A. Rehn

BACKGROUND

The major objective of this study was to gain a greater understanding of the theory and operation of inert-gas hollow cathodes, and thereby facilitate the achievement of long operating lifetimes. A secondary objective was ease and reliability of starting. Both argon and xenon were of interest for possible future missions, although argon was emphasized because it represents a greater departure from the usual thruster propellants of cesium and mercury. Other inert-gas propellants were also used to give additional insight into hollow cathode operation.

During the previous support period of this grant the hollow cathode configuration consisted of a thermionic emitter inside a cathode chamber of several centimeters diameter.[1] Such an internal emitter permitted reproducible emission characteristics without the coating and conditioning problems of barium strontium oxides. An internal emitter also facilitated starting without high voltage, and should have a longer lifetime inside a hollow cathode than exposed to the ion-chamber discharge. The use of a bias voltage between the internal emitter and the cathode chamber was found to extend the operating range and eliminate plasma fluctuations, as well as facilitate reliable starting.

The lifetime limitation for a hollow cathode results from the erosion caused by ions from the surrounding plasma falling back on the orifice region. Because of this erosion problem, improvements in hollow-cathode performance have been directed at either a reduced coupling voltage for a given emission or an increased emission for a given coupling voltage.

For long lifetimes, the coupling voltage should be low enough to reduce the energy of the bombarding ions below the threshold value. For tungsten, the threshold energy ranges from about 25 to 35 eV for neon, argon, krypton, xenon, and mercury ions, with an uncertainty of perhaps 5 eV for data with any one of these ions.[2,3]

During this last year, argon neutralizer tests with an operating thruster were conducted first by Sovey[4] and later as part of this grant activity. These tests gave consistently lower coupling voltages (hence longer expected lifetimes) than had been obtained in bell jar tests. This result was unexpected in that the bell jar tests had been conducted with configurations that had given an acceptable simulation of thruster operation with mercury propellant. The resolution and understanding of the differences between bell jar and operating thruster tests was a major aspect of the hollow cathode work during this last year. In addition to tests in both bell jar and thruster environments, the two cathode types shown in Fig. 2-1 were investigated. The conventional hollow cathode type (Fig. 2-1 (a)) is similar to configurations used for many years with mercury propellant, while the internal emitter type was explored during the previous support period of this grant. As the differences between bell jar and thruster operation became better understood, the differences in the two environments were found to be more important than the differences in the two cathode types. The emphasis therefore shifted to the conventional cathode type, which is more suited to flight applications.

APPARATUS AND PROCEDURE

The conventional hollow cathodes that were tested (Fig. 2-1 (a)) were all fabricated of 6.35-mm diameter tantalum tubing with a matching tip of 1-mm thick thoriated tungsten. Ten-ampere swaged heater wire was wrapped

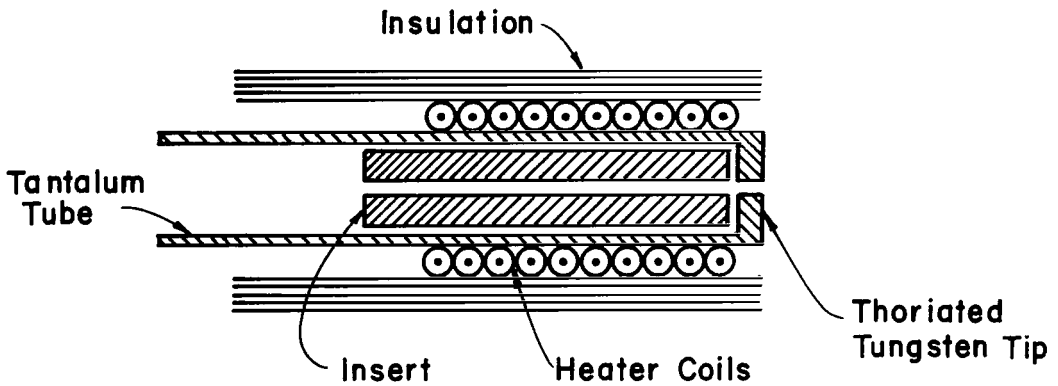

(a) Conventional Hollow Cathode

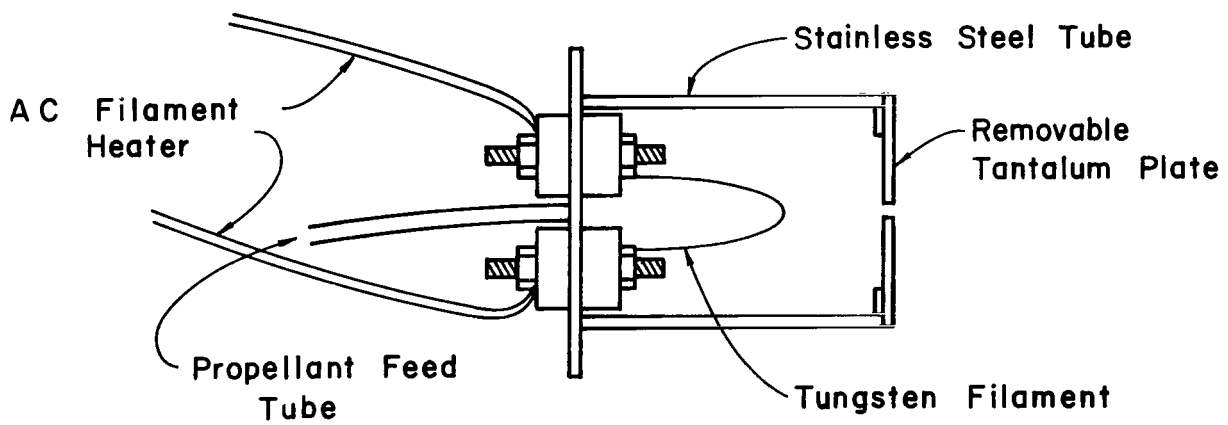

(b) Hollow Cathode with Internal Emitter

Figure 2-1. Hollow cathode types used in investigation.

for about 1 cm near the tip and covered with tantalum foil to reduce the radiation heat loss. The inserts were close fitting porous tungsten cylinders 13 mm long with 2.5 mm holes through the axis. These inserts were impregnated with a mixture of barium and strontium oxides. A small quantity of this oxide mixture was added when starting became difficult due to air entering the feed line. (This problem was subsequently solved by a more careful purging technique.) Radiation fins, when used, were 17 mm in diameter and 0.5 mm thick. They were made of tantalum and were electron-beam welded to the outside edge of the cathode tip. Orifice sizes used in the conventional hollow cathodes were 0.41, 0.61, and 0.79 mm. The first two were straight cylindrical holes, while the last was chamfered at the downstream end.

The internal emitter type of hollow cathode was varied slightly in diameter for different tests, but was always within the broad optimum of 2 to 3 cm determined in previous tests.[1] The side wall and back plate of this cathode were made of 1.5 mm thick stainless steel, while the orifice plate was made of 1.0 mm tantalum. Although various orifice sizes were studied in earlier investigations, only data for a 2-mm orifice are included here. The internal emitter was a loop of 0.25-mm diameter tungsten wire, which had a total length of 3 to 4 cm.

Initial bell jar testing of the internal emitter type of cathode employed a 15-cm thruster simulator in an attempt to duplicate the operating environment of the main cathode. (An electrical block diagram for the thruster simulator and the other two basic cathode configurations is shown in Fig. 2-2.) The use of a stainless steel screen 2.5 cm downstream of the orifice decreased the cathode coupling voltage, but not enough to approximate actual operating conditions for either discharge-chamber or neutralizer

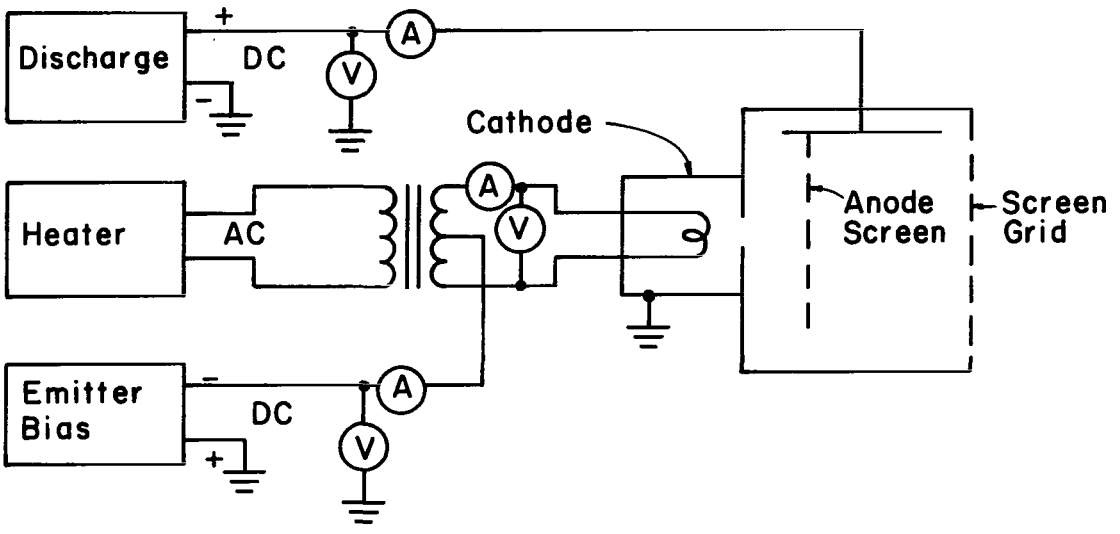

(a) Bell jar thruster simulator configuration.

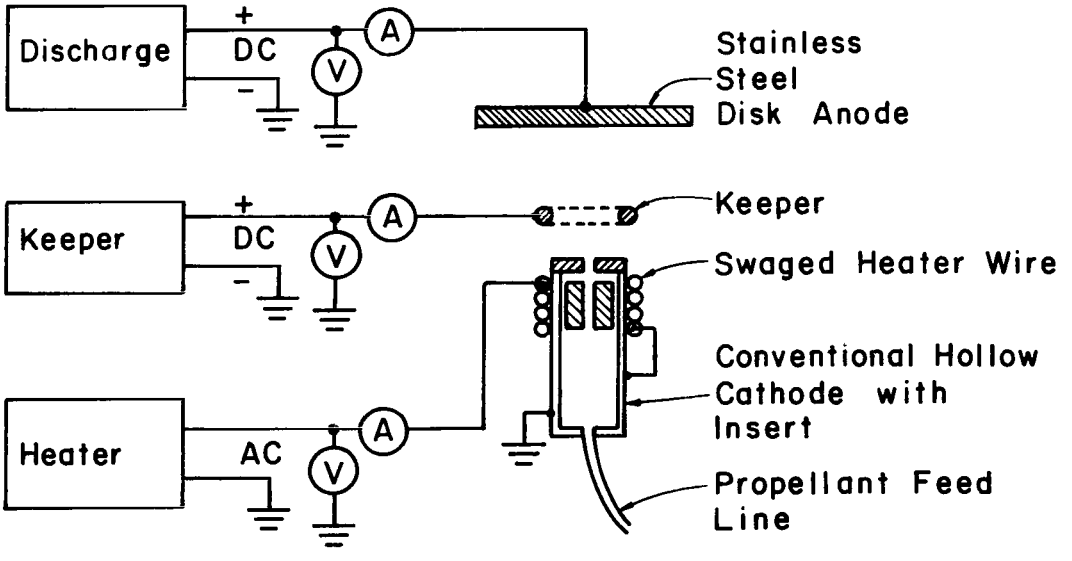

(b) Bell jar diode configuration.

Figure 2-2. Electrical block diagram.

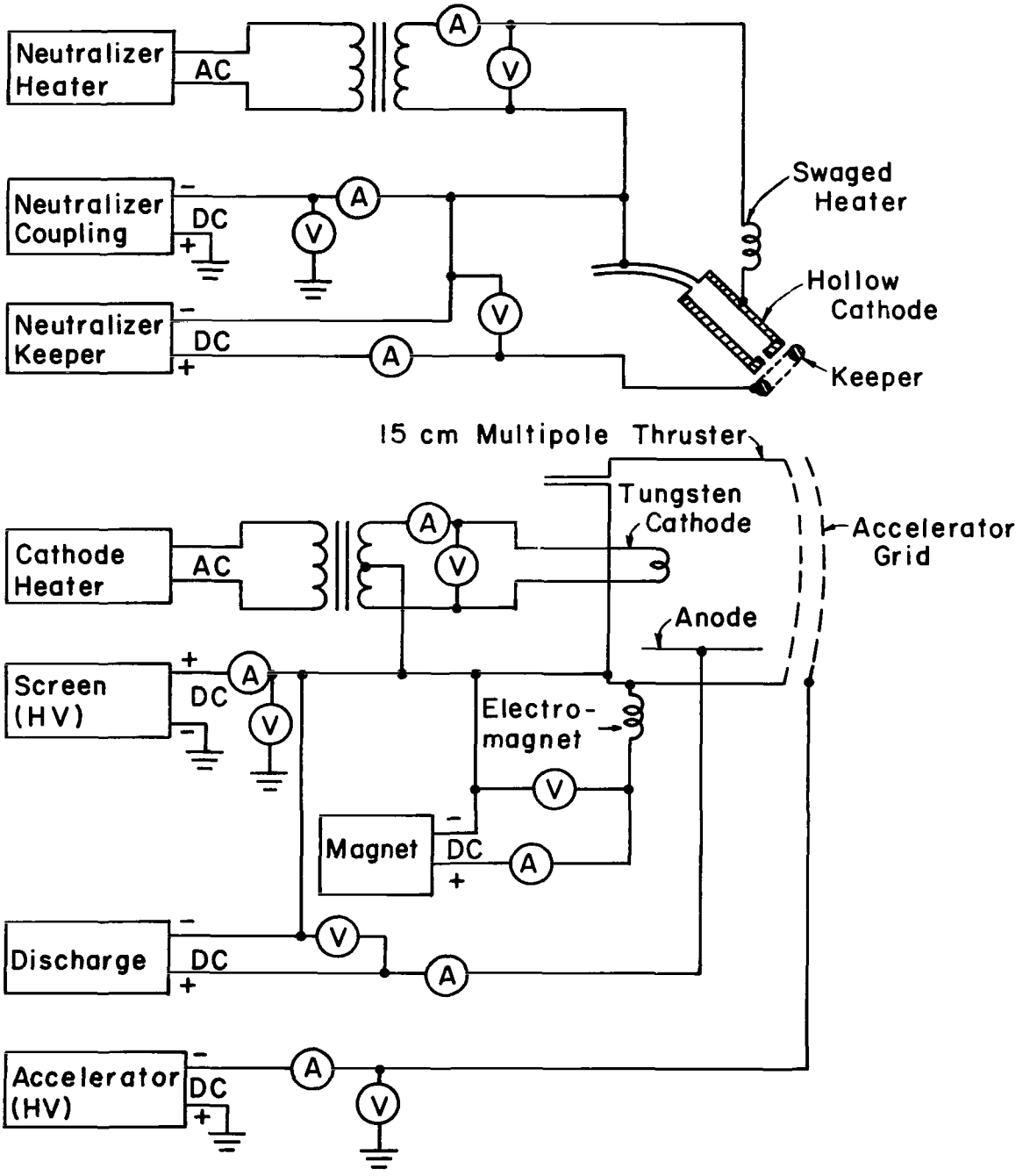

(c) Neutralizer configuration.

Figure 2-2. Concluded.

cathodes. A more complete description of this thruster simulator can be found in the preceding annual report.[1]

Later bell jar tests used stainless steel disks for the anode (without the thruster simulator). (See Fig. 2-2(b).) These disks were 2 to 3 cm in diameter and 1.6 mm thick. Data are presented herein for anode-cathode separations of 4.25 mm and 10 mm.

The neutralizer tests were conducted in the 1.2-m diameter vacuum facility. (See Fig. 2-2(c).) A 15-cm multipole thruster with an 8.1-cm long chamber was used for all neutralizer tests. This thruster is described in the preceding annual report. A beam current of 250 mA was used for all tests. When argon was used as the propellant, the total neutral flow to the thruster was kept constant at 400 mA-equivalent. The location of the neutralizer relative to the thruster accelerator system is indicated in Fig. 2-3. Although the internal emitter type of cathode is shown in Fig. 2-3, the orifice of the conventional hollow cathode (when used) was placed in the location shown for the orifice of the internal emitter type.

Langmuir probes were used to determine plasma properties in some of the tests. In the bell jar the probe was 0.64-mm diameter tantalum wire, exposed for a 2 mm length. The probe location in these tests was midway between the cathode orifice and the anode disk. The probe for the neutralizer tests was the same, except that a 1-cm exposed length was used. The location in the neutralizer tests was at the center of the beam, 5 cm downstream of the accelerator grid. In both cases the Debye length was comparable to the probe diameter, so that a thick-sheath probe analysis was necessary.[5]

A heater current of 7 amperes was used for the internal emitter cathode. During long runs in the bell jar, heater current adjustments were made to

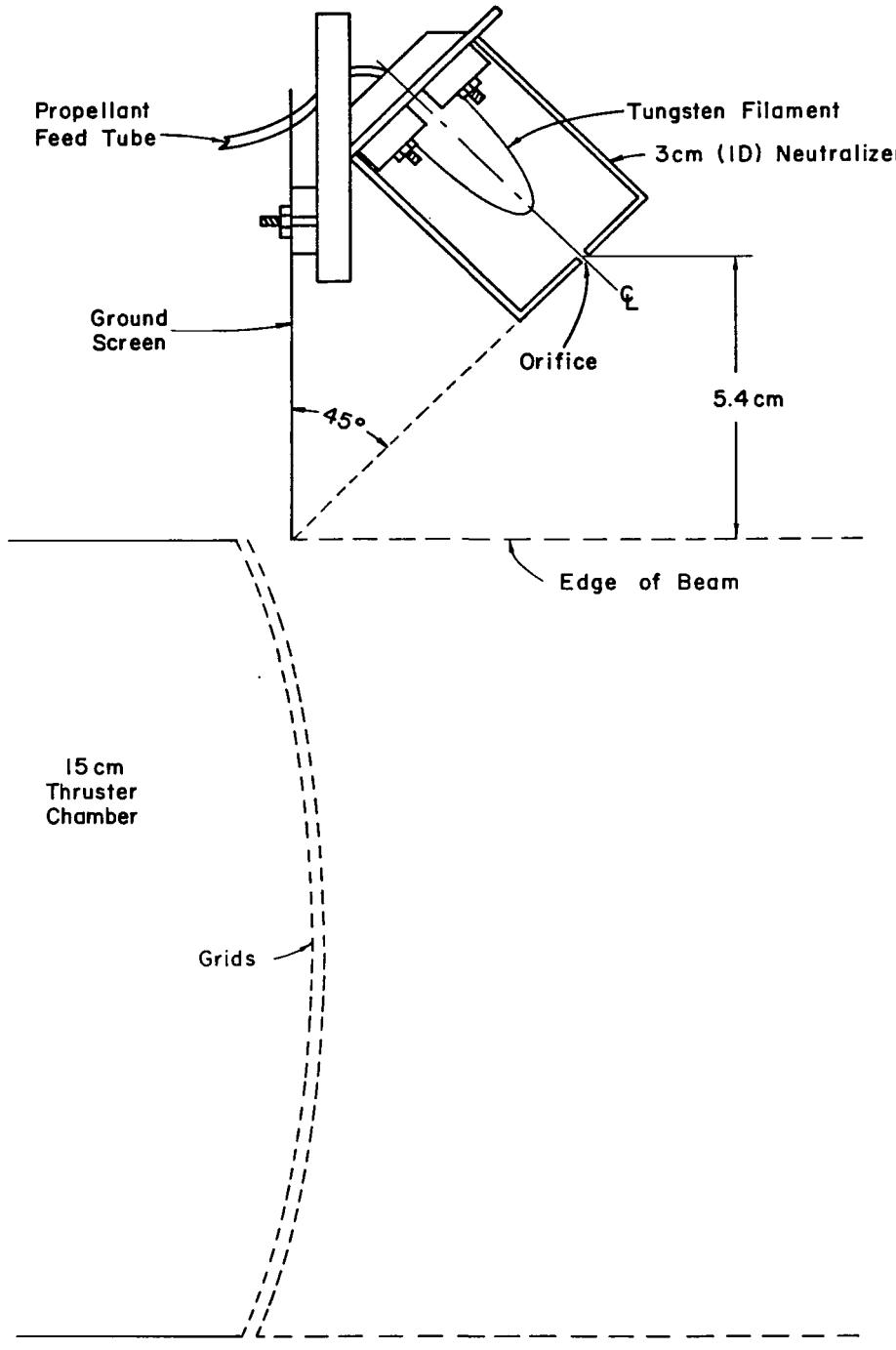

Figure 2-3. Internal emitter hollow cathode in the neutralizer configuration.

maintain a standard bias current when operated in the bias mode. This procedure has been described previously.[1] The equivalent emission calibration for the conventional hollow cathode was established with a temperature measurement, as explained later. An optical pyrometer was used to determine the temperature of the tip near the orifice. The absolute accuracy of these temperature measurements was limited by the usual problem of viewing through thick glass, but the repeatability of measurements was within about ± 5°C.

EXPERIMENTAL RESULTS

Internal Emitter Hollow Cathode

The performance of the internal emitter hollow cathode is shown in Fig. 2-4 for several propellant flow rates. The disk anode was used for these data, with an anode-cathode spacing of 4.25 mm. The chamber diameter of this cathode was 2.5 cm in diameter and a 2 mm orifice was used. The cathode body was at ground potential in the test configuration used. The discharge voltage V_d was the positive potential of the anode relative to ground. (The emitter was heated with alternating current. "Emitter potential" was the centertap potential of the heater-transformer secondary.) This type of cathode therefore had a bias current I_b (emitter to cathode body) in addition to the discharge current I_d (cathode body to anode).

As shown in Fig. 2-4, the discharge voltage at a given discharge current decreased with increasing propellant flow. This general performance trend was typical of all hollow cathodes tested so far. The curve shapes tended to remain the same for different anode-cathode spacings, but shifted to higher voltages for larger spacings. The shape of the curves shown in Fig. 2-4 was

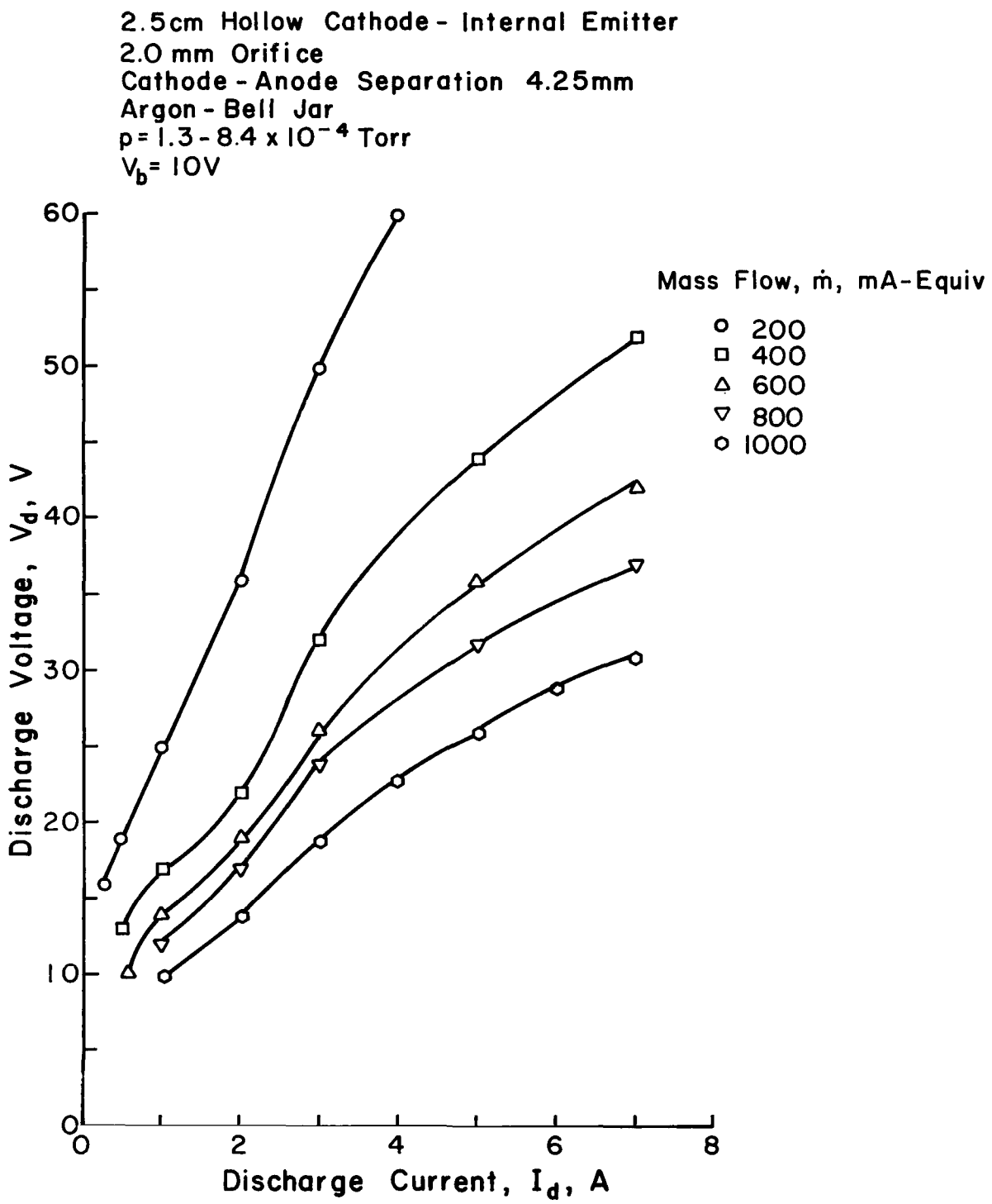

Figure 2-4. Effect of propellant flow rate changes for an internal emitter hollow cathode with a stainless steel disk anode.

also typical for bell-jar operation with a disk anode, in that the current-voltage characteristic for a fixed propellant flow rate could be approximated by a straight line over most of the range investigated.

The performance of the internal emitter cathode when used as a neutralizer is shown in Fig. 2-5. (The configuration shown in Fig. 2-3 was used for this test.) The orifice size was 2 mm, while the cathode-chamber diameter was 3 cm. The latter was slightly larger than the 2.5 cm used for the data in Fig.2-4, but this difference was not enough to give any significant change in performance. Equipment limitations with these data also limited the coupling current to about 1 ampere. The curve shapes shown, though, are typical of neutralizer tests. The coupling voltage at a given coupling current decreased with increasing propellant flow. This decrease in coupling voltage was largest between 200 and 300 mA-equivalent. At, or above, 300 mA-equivalent the curves were somewhat "S" shaped, with a central plateau in which small changes in coupling voltage gave large changes in current. The "S" shaped curves were typical for neutralizer operation at high propellant flow rates, and have also been observed in many previous tests with the 15-cm thruster simulator.[1]

In the configuration used for the neutralizer tests the cathode is biased negative relative to the vacuum facility. The voltage difference between the cathode and the facility is the coupling voltage V_{cf} shown in Fig. 2-5. Because the ion beam is more positive than the vacuum facility, there is still a voltage difference between the cathode and the ion beam at a zero value of V_{cf}. Nonzero coupling currents were therefore observed at zero coupling voltage in Fig. 2-5.

A comparison of internal emitter cathode performance as a neutralizer and with the 15-cm thruster simulator is shown in Fig. 2-6. The operating

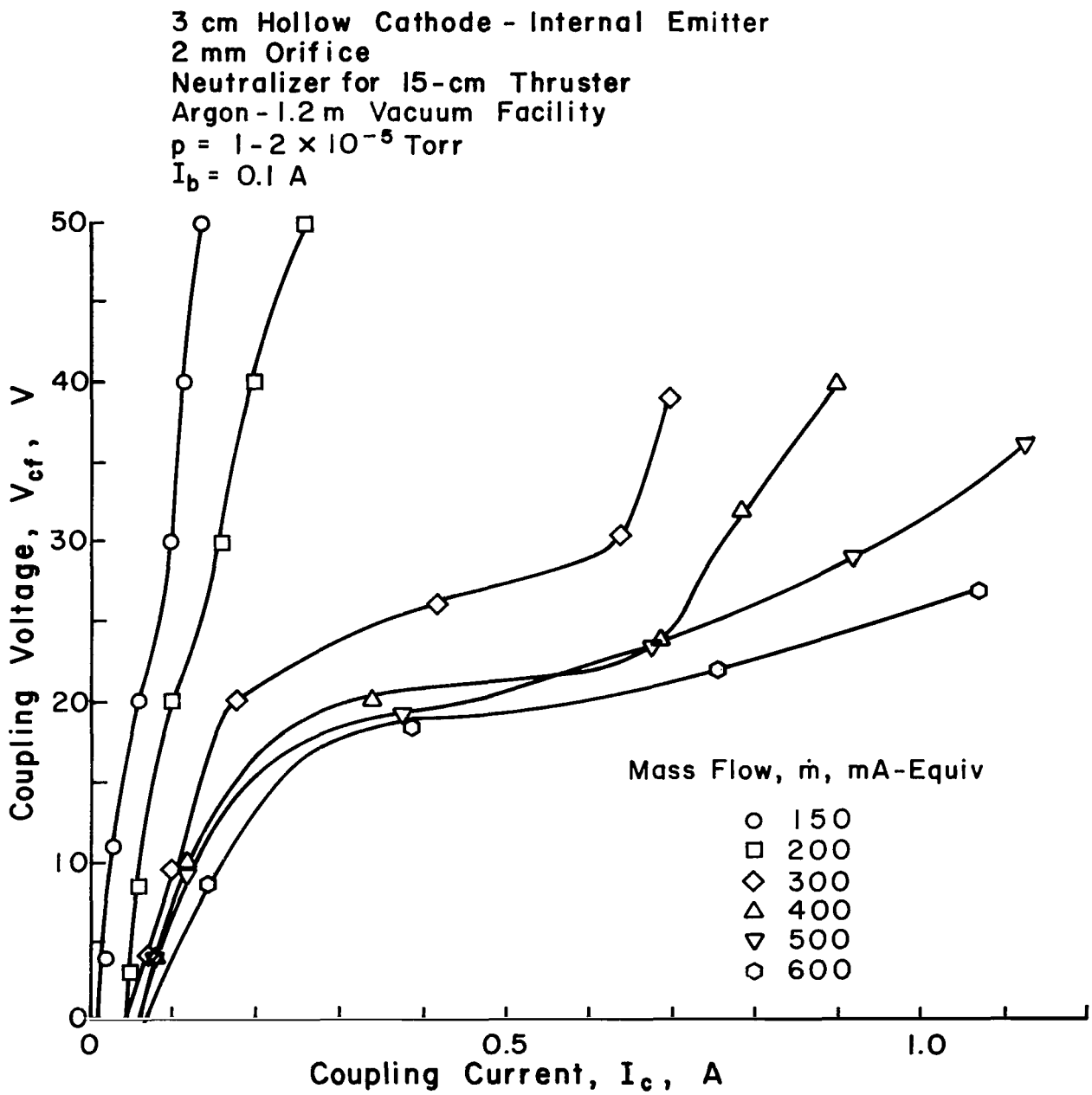

Figure 2-5. Effect of propellant flow rate changes for an internal emitter hollow cathode in the neutralizer configuration.

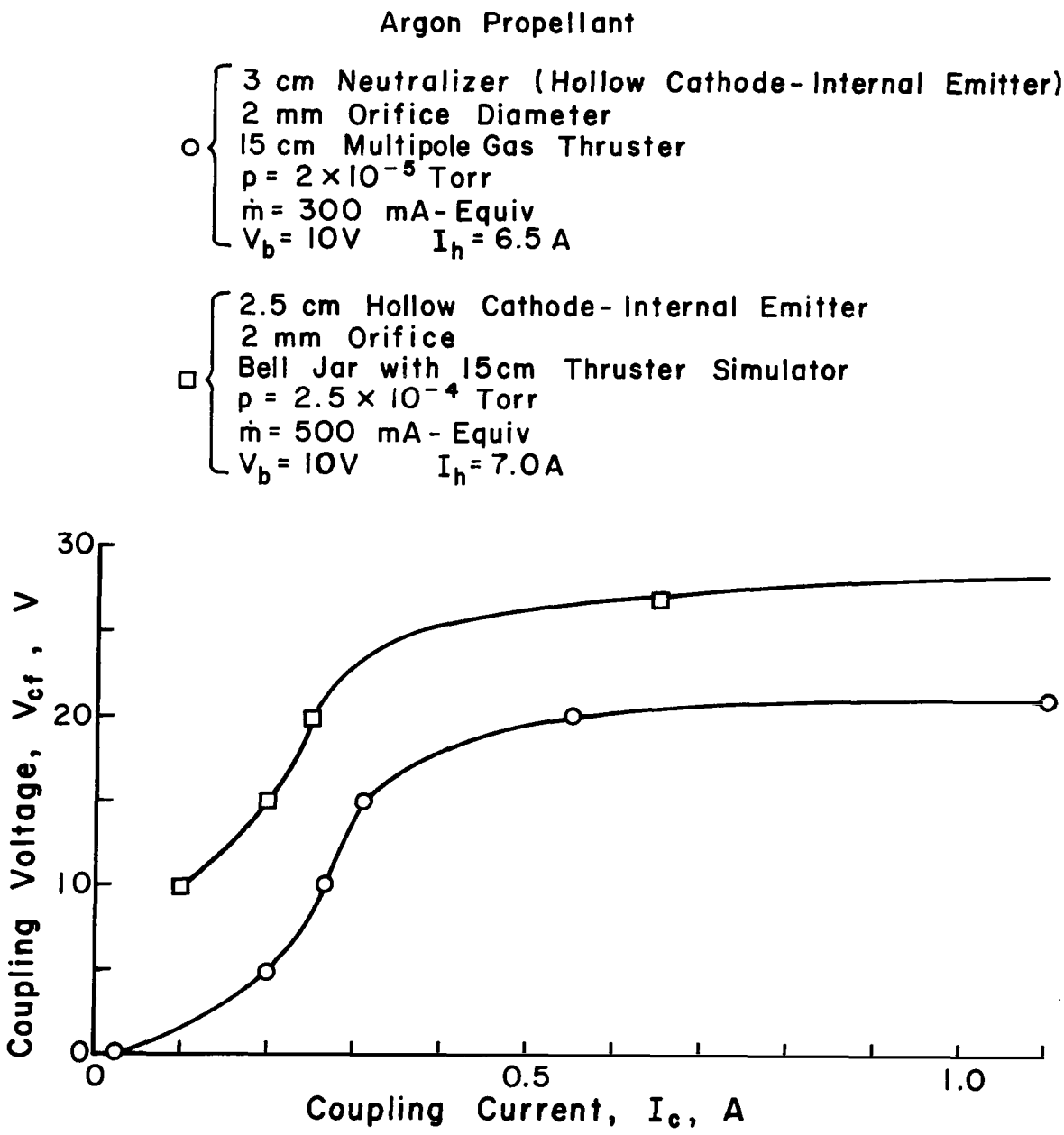

Figure 2-6. Comparison of internal emitter hollow cathode performance as neutralizer and in 15-cm thruster simulator.

conditions are not precisely the same, but the similarity of curve shape is clearly evident. Despite a lower propellant flow rate, the neutralizer cathode operated at 7 to 10 V lower in coupling voltage. The coupling voltage for the neutralizer was defined as described above, so therefore does not include the potential difference between the ion beam and the vacuum facility. The coupling voltages for neutralizer operation, though, approximate the values found acceptable for mercury propellant neutralizers, while the coupling voltages for thruster-simulator operation are too high over most of the operating range. The results shown in Fig. 2-6 are typical of all comparisons between neutralizer and thruster-simulator operation.

Conventional Hollow Cathode

The performance of a conventional hollow cathode with a disk anode is shown in Fig. 2-7 for several krypton flow rates. Similar to the data shown in earlier curves, the voltage at a constant current tends to decrease as propellant flow rate is increased. The data of Fig. 2-7 were also selected to show double valued voltages for a single current. Similar double valued performance has been observed several times and is believed to be a real effect rather than a data error.

The data for each mass flow rate in Fig. 2-7 were obtained at a constant tip temperature. The choice of a constant temperature value was not completely arbitrary because a cathode would usually operate over only a limited range. The usual procedure for setting tip temperature was to use a mean value for a range of heater powers and discharge currents. This mean value was then held constant by varying the heater power as discharge current was varied.

A comparison between bell-jar and neutralizer operation is shown in Fig. 2-8. Note that the coupling voltage is again higher for the bell-jar operation, despite a higher propellant flow rate for those data. Similar to

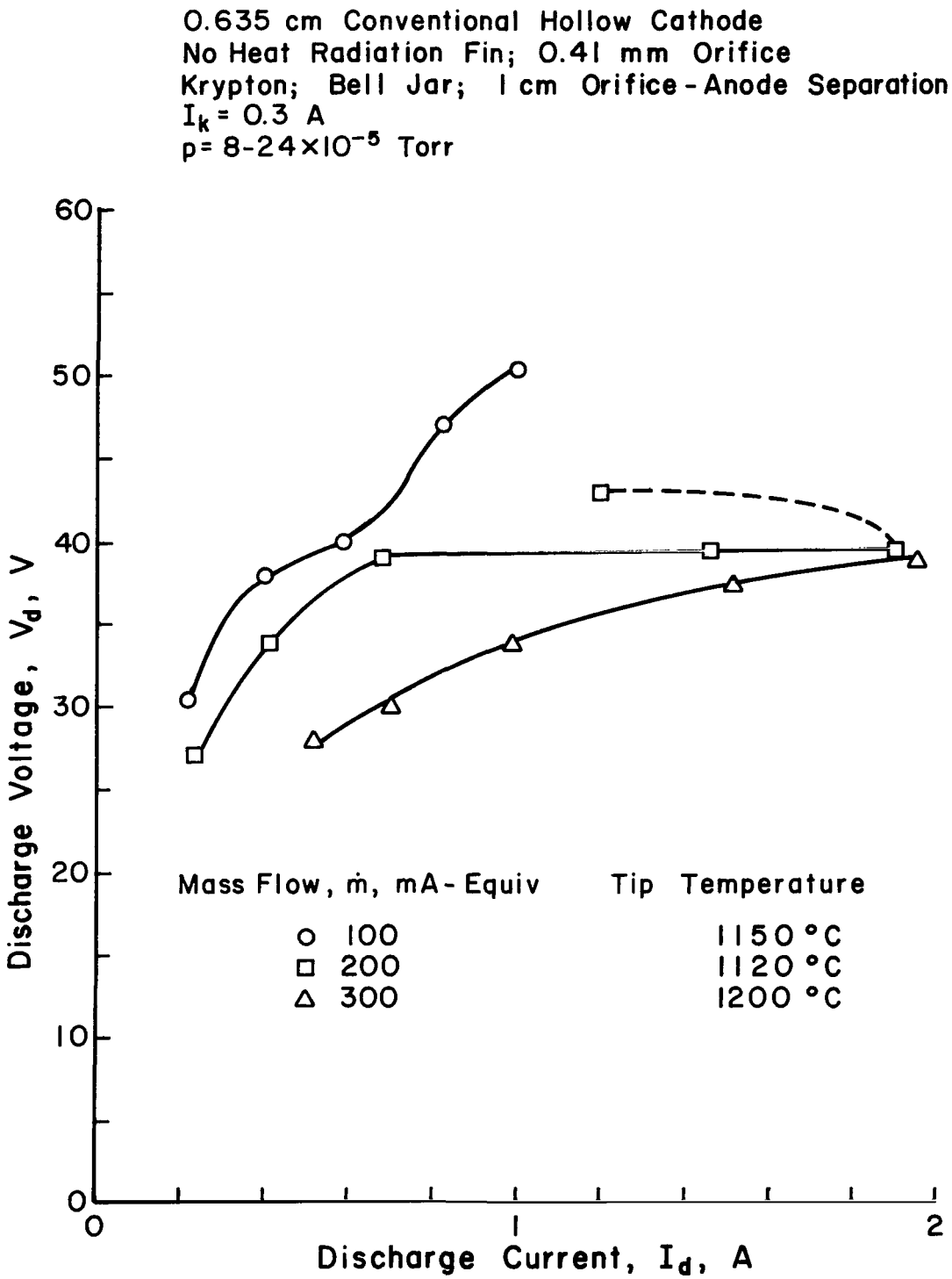

Figure 2-7. Effect of propellant flow changes for a conventional hollow cathode with a stainless steel disk anode.

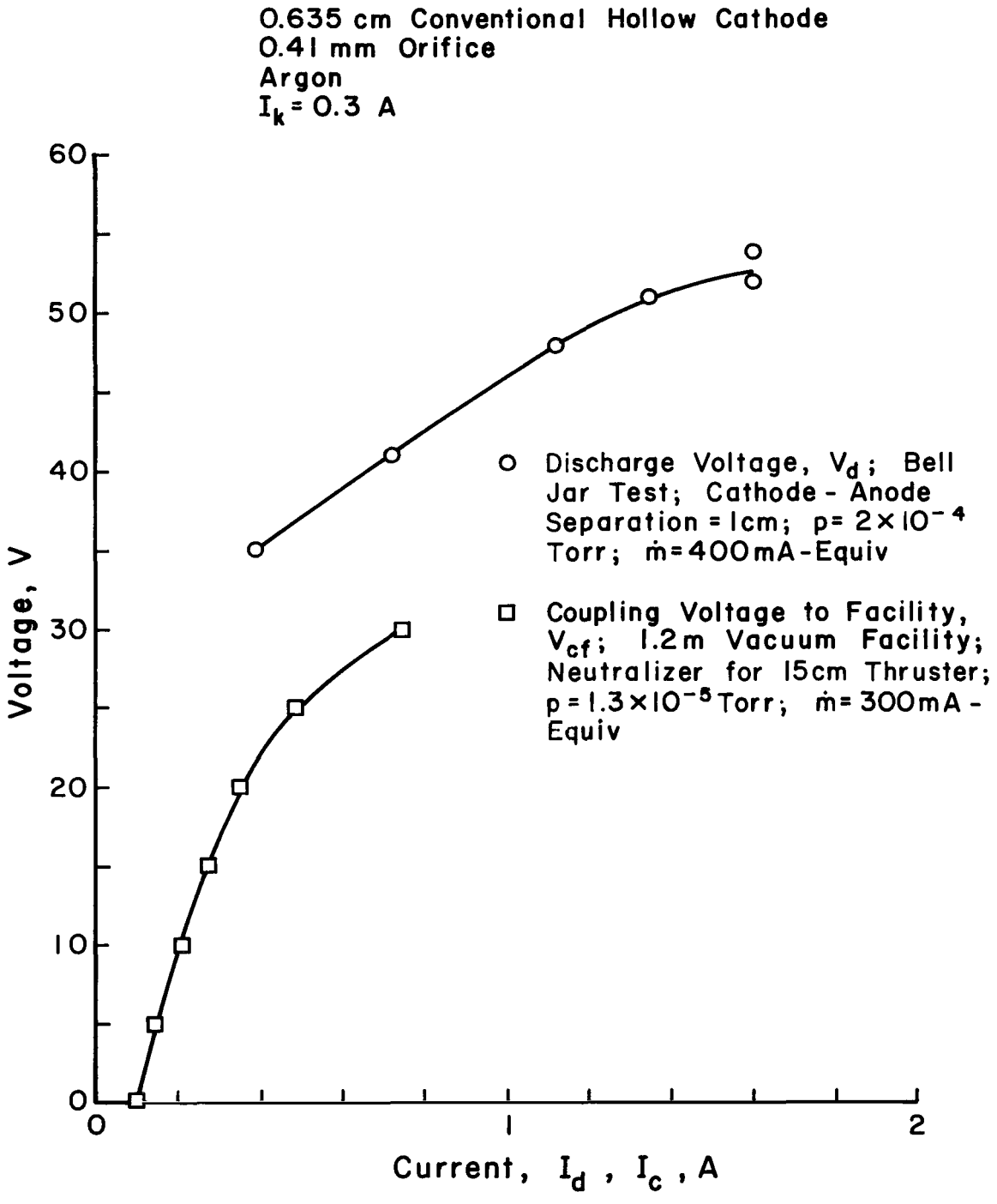

Figure 2-8. Comparison of bell-jar and neutralizer performance for a conventional hollow cathode.

the earlier observation with internal emitter cathodes, a nonzero neutralizer coupling current was observed at zero coupling voltage (V_{cf}).

The effect of varying keeper current is shown in Fig. 2-9 for one propellant flow rate. There is a clear trend to higher coupling current and lower coupling voltage as the keeper current is increased. Although this trend continued at higher keeper currents, the keeper became very hot (incandescent) at, or above, 0.4 A. As a result most subsequent tests were conducted at a keeper current of 0.3 A.

The data of Fig. 2-9 were obtained at constant heater power, with the tip temperature allowed to vary. Most of the same data are shown in Fig. 2-10, together with the corresponding tip temperatures. The tip temperature increases continuously with increasing coupling voltage and current for keeper currents of both 0.13 and 0.3 A. For a keeper current of 0.4 A, however, the tip temperature reaches a minimum between coupling currents of 0.1 and 0.2 A. It is significant that the range of temperatures shown in Fig. 2-10 has been shown to be consistent with long insert life in studies conducted by Wilbur.[6]

Data from another study involving cathode temperature are shown in Fig. 2-11. The cathode used had a heat radiation fin and was operated at nearly constant tip temperature by varying heater power from 0 to 150 W. The tip temperature is shown by the upper curve. The voltage-current performance as a neutralizer is shown by the middle curve. Note that the double valued curve shown is similar to that discussed in connection with Fig. 2-7. The use of a heat radiation fin and a larger orifice permitted significantly larger coupling currents for a given temperature (Fig. 2-11 versus Fig. 2-10), but an increase in propellant flow rate is probably also required. The lower curve in Fig. 2-11 shows the variation of heat fin temperature, which roughly

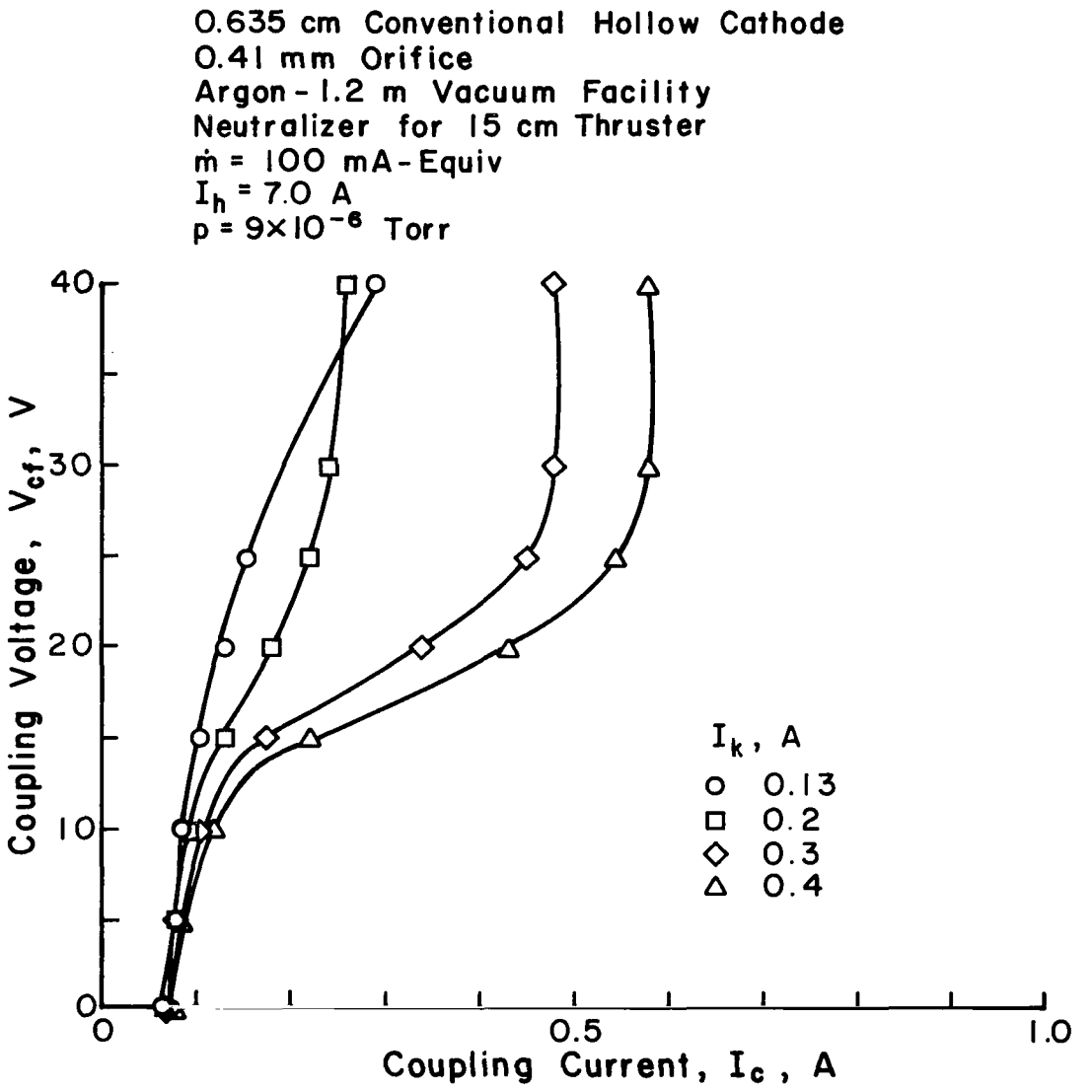

Figure 2-9. Effect of keeper current for a conventional hollow cathode operated as a neutralizer.

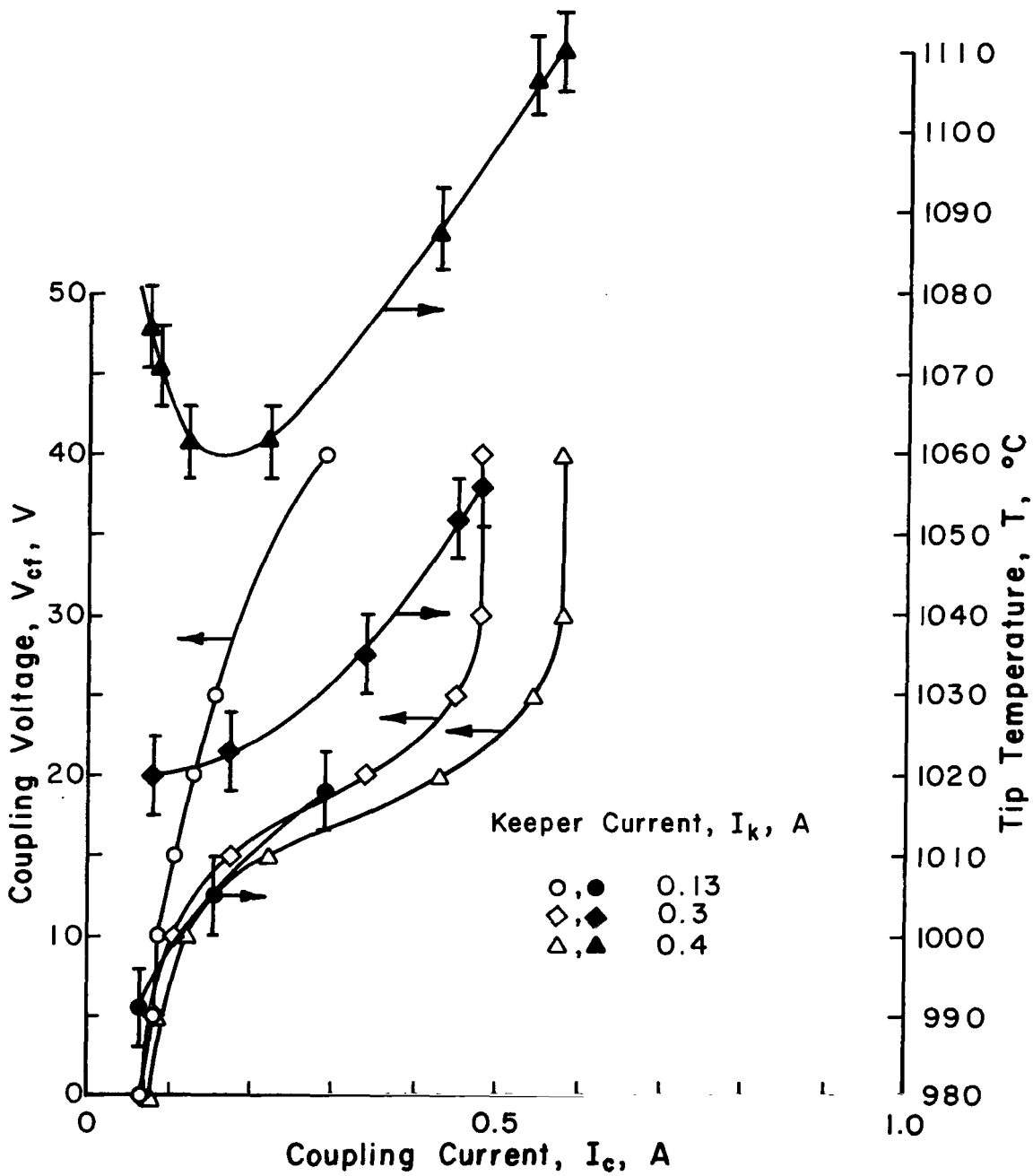

Figure 2-10. Conventional hollow cathode performance and tip temperatures. Constant cathode heater power.

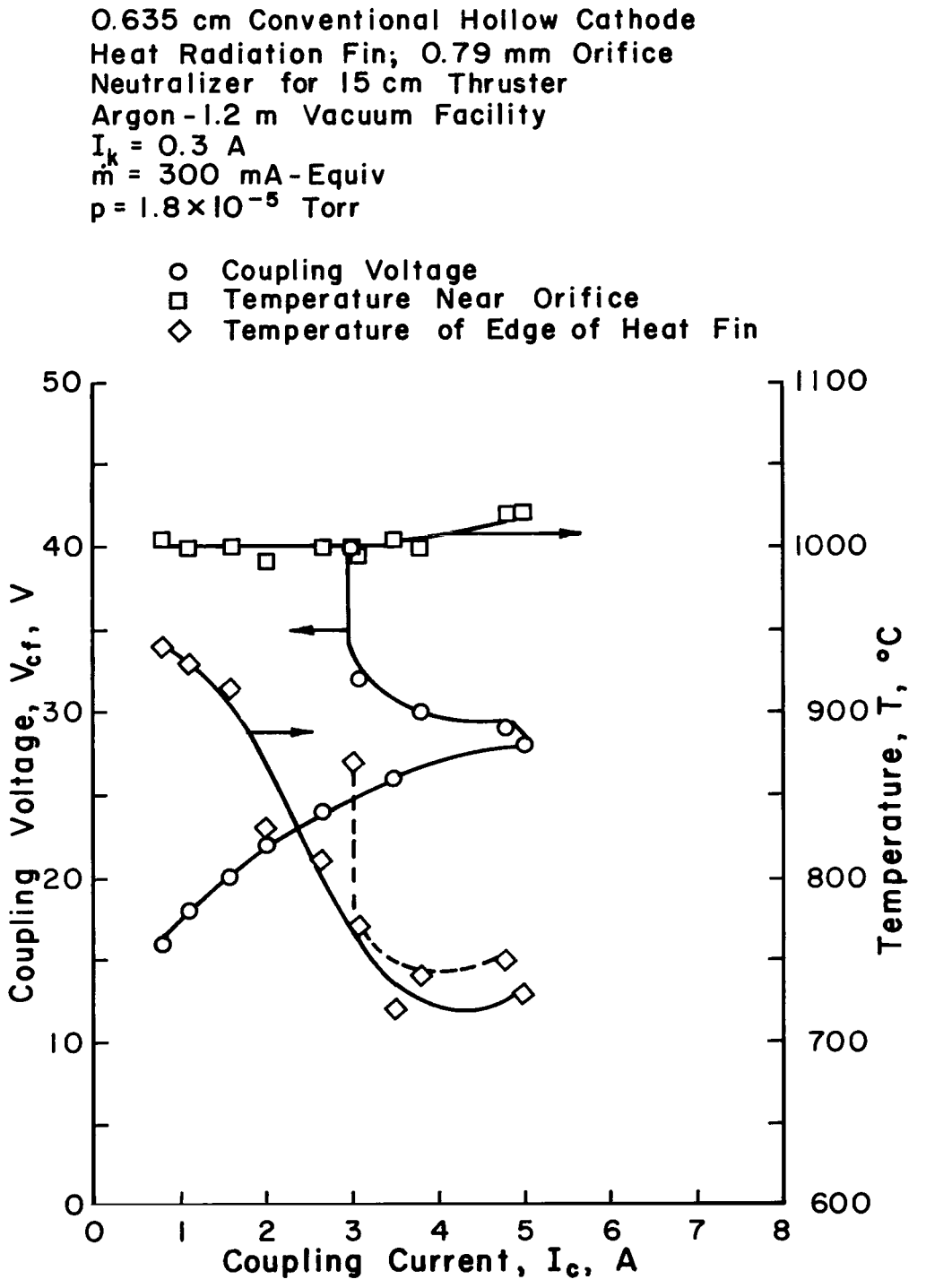

Figure 2-11. Conventional hollow cathode with a heat radiation fin. Tip temperature held nearly constant.

follows the variation in heater power. Because of the T^4 relationship for radiation, the heat fin can play an important role in maintaining the proper tip temperature. At a coupling current of 5 A, the discharge power (coupling current times coupling voltage) was 140 W. Most of this power is probably absorbed by the tip--without raising the tip to an excessive temperature.

Neutralizer performance for several propellant flow rates is shown in Fig. 2-12. As shown before, there is a general trend towards decreased coupling voltage and increased current for an increase in propellant flow rate. Note that the tip temperatures cover a range of only 70°, except for the 50 mA-equivalent flow rate. The higher temperature was required for stable operation at this low flow rate. In general, operation at marginal conditions required higher tip temperatures.

To summarize the effects of the different conventional hollow cathode configurations, both heat fins and larger orifices clearly raise the current capacity at a given tip temperature. An increase in orifice diameter should also be accompanied by an increase in propellant flow rate if the full benefit of the larger orifice is to be obtained. These effects of heat fins and orifice size are all consistent with previous experience using mercury propellant.

Plasma Coupling Voltage

Proper simulation of cathode operation in a thruster has been a recurrent problem in the study of inert-gas hollow cathodes. Such simulation is desirable because bell-jar operation uses less manpower and equipment, hence permits a broader investigation with the same total resources. The comparisons shown in Figs. 2-6 and 2-8, however, clearly show that the same or similar cathodes can give significantly different performance for different test environments.

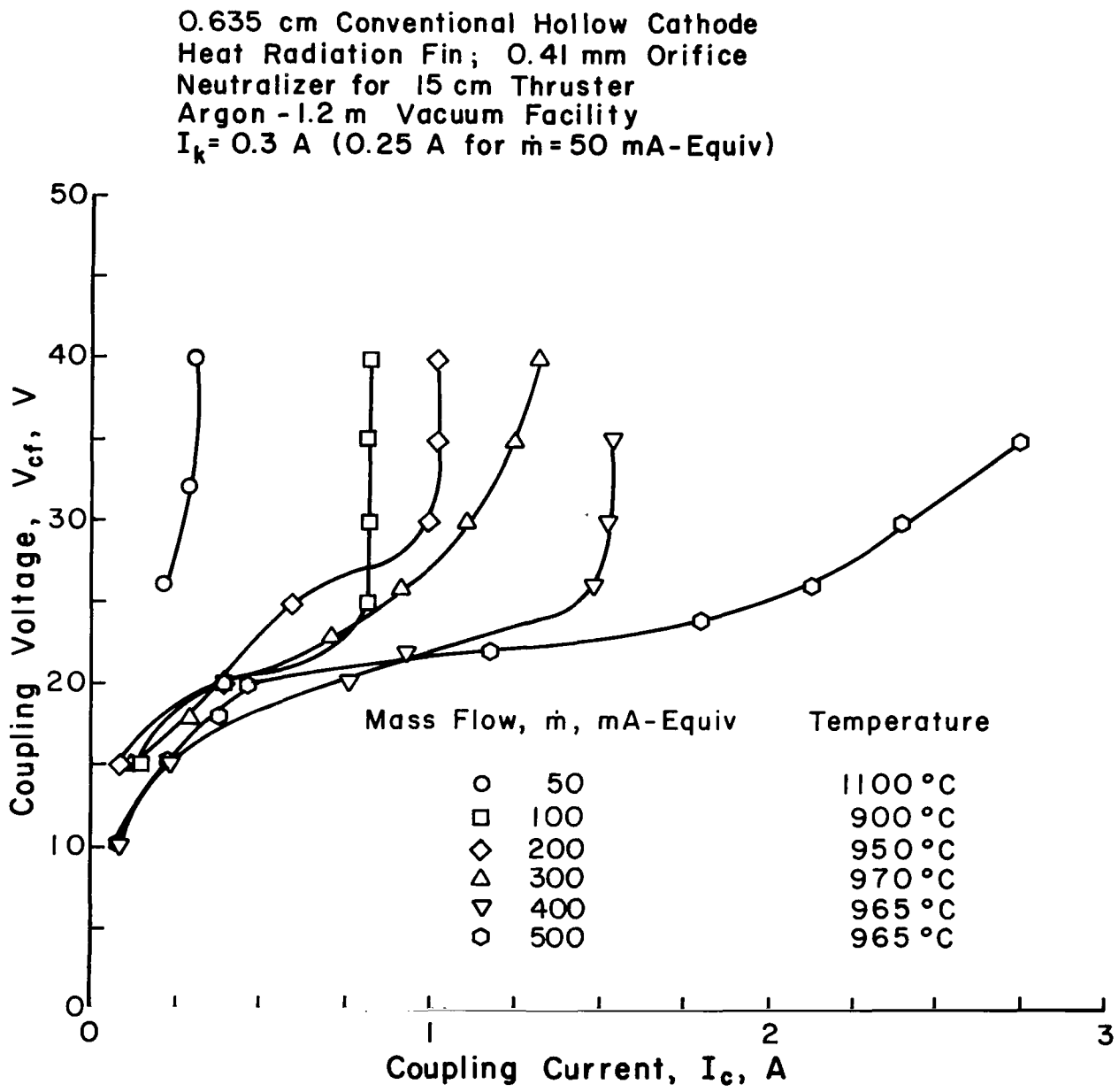

Figure 2-12. Effect of propellant flow rate on neutralizer performance of a conventional hollow cathode.

In order to better understand the problems of simulating cathode performance in a thruster, a number of plasma probe measurements were made. The coupling voltage between a conventional hollow cathode and the vacuum facility (neutralization configuration) is shown in Fig. 2-13 for one propellant flow rate. (The data shown for this curve are the same as the 400 mA-equivalent data shown in Fig. 2-12.) Also shown in Fig. 2-13 is the coupling voltage between the cathode and the plasma potential at the center of the ion beam. This plasma potential is positive relative to the facility, so that the coupling voltage to the plasma is the sum of the plasma potential and facility coupling voltage. Both curves of coupling voltage show the same general shape. As indicated earlier, the larger coupling voltage to the plasma permits the cathode to emit at zero coupling voltage to the facility (Figs. 2-8 through 2-10). Inasmuch as the center of the ion beam close to the thruster is the most positive plasma potential in the beam, this location can also be used to define the maximum ion energy for cathode erosion. The number of ions from this location that reach the cathode, though, is probably very small. Acceptable lifetimes should therefore be obtained with plasma coupling voltages somewhat above the sputtering threshold. From the plasma coupling voltages shown, the neutralizer configuration used should show long lifetimes for neutralization currents up to about 1 ampere.

The same conventional hollow cathode configuration as used for Fig. 2-13, except without a radiation heat fin, was operated with krypton propellant. In the neutralizer configuration, Fig. 2-14, the plasma and facility coupling voltages again show similar curve shapes. As with argon, the plasma coupling voltage is larger than the facility coupling voltage.

The same cathode as used for Fig. 2-14 was also tested in a bell jar with a disk anode. As shown in Fig. 2-15, the plasma coupling voltage was substantially less than the discharge voltage. (In this case the plasma coupling

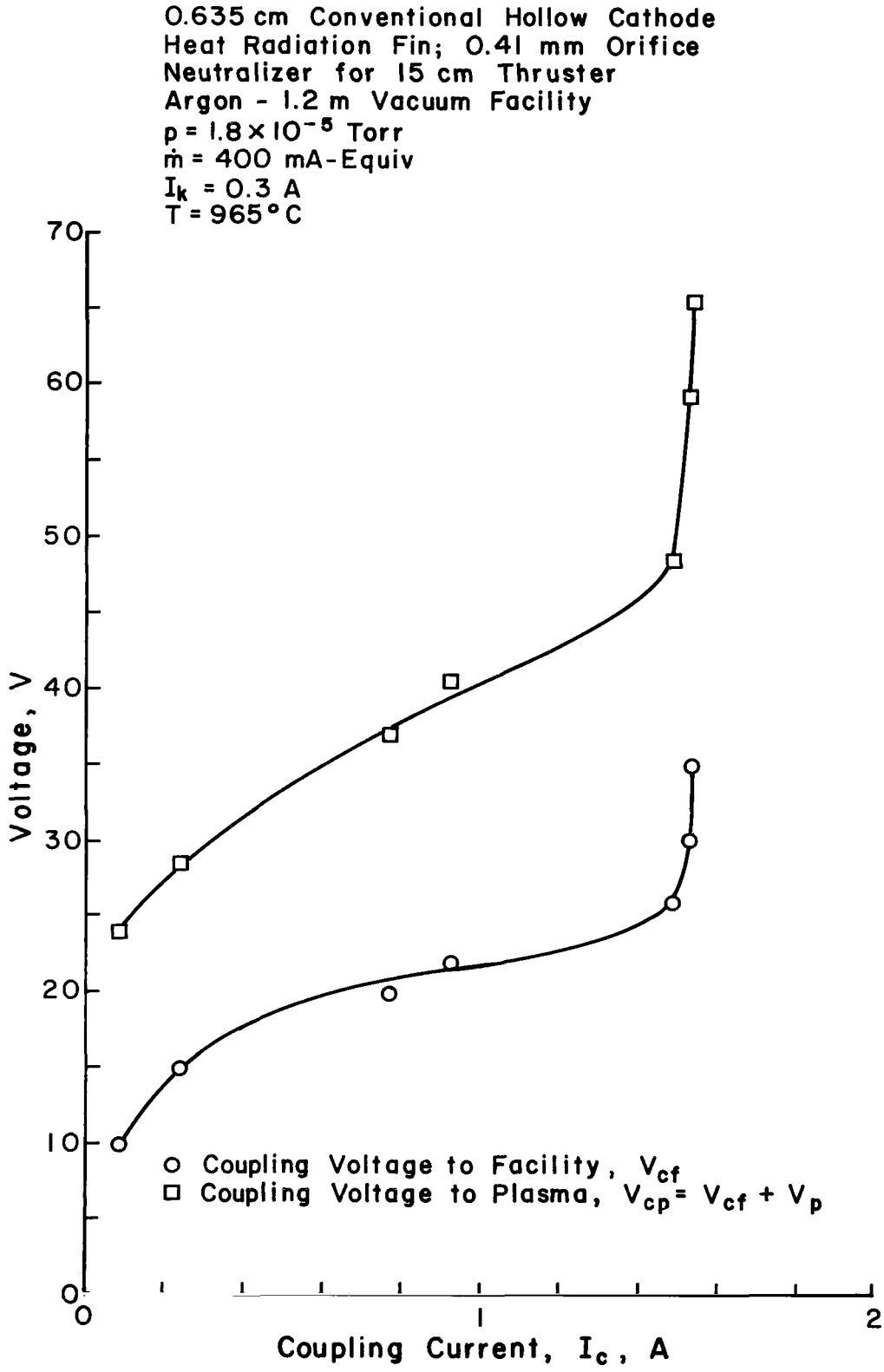

Figure 2-13. Comparison of facility coupling voltage with plasma coupling voltage. Neutralizer configuration with argon propellant.

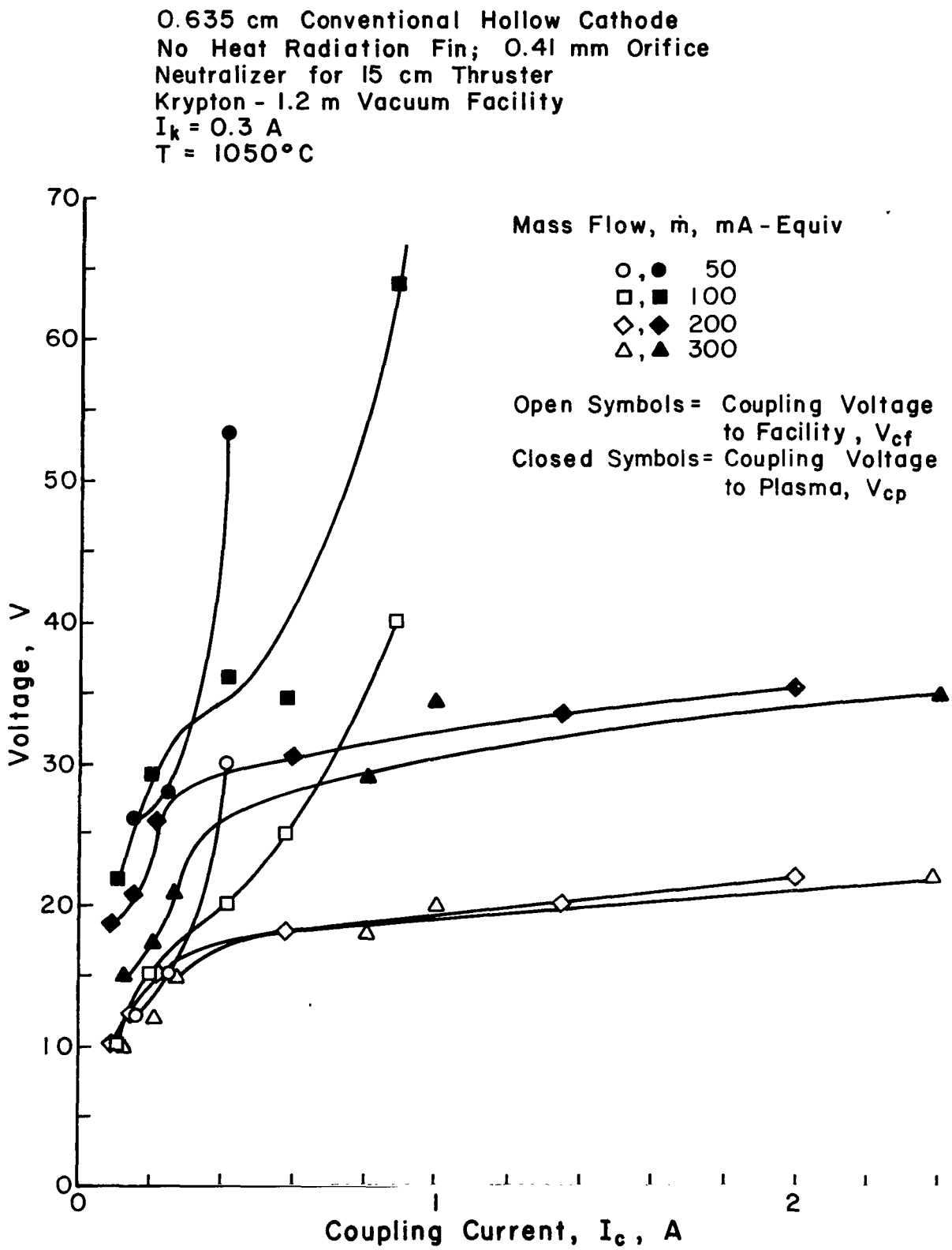

Figure 2-14. Comparison of facility coupling voltage with plasma coupling voltage. Neutralizer configuration with krypton propellant.

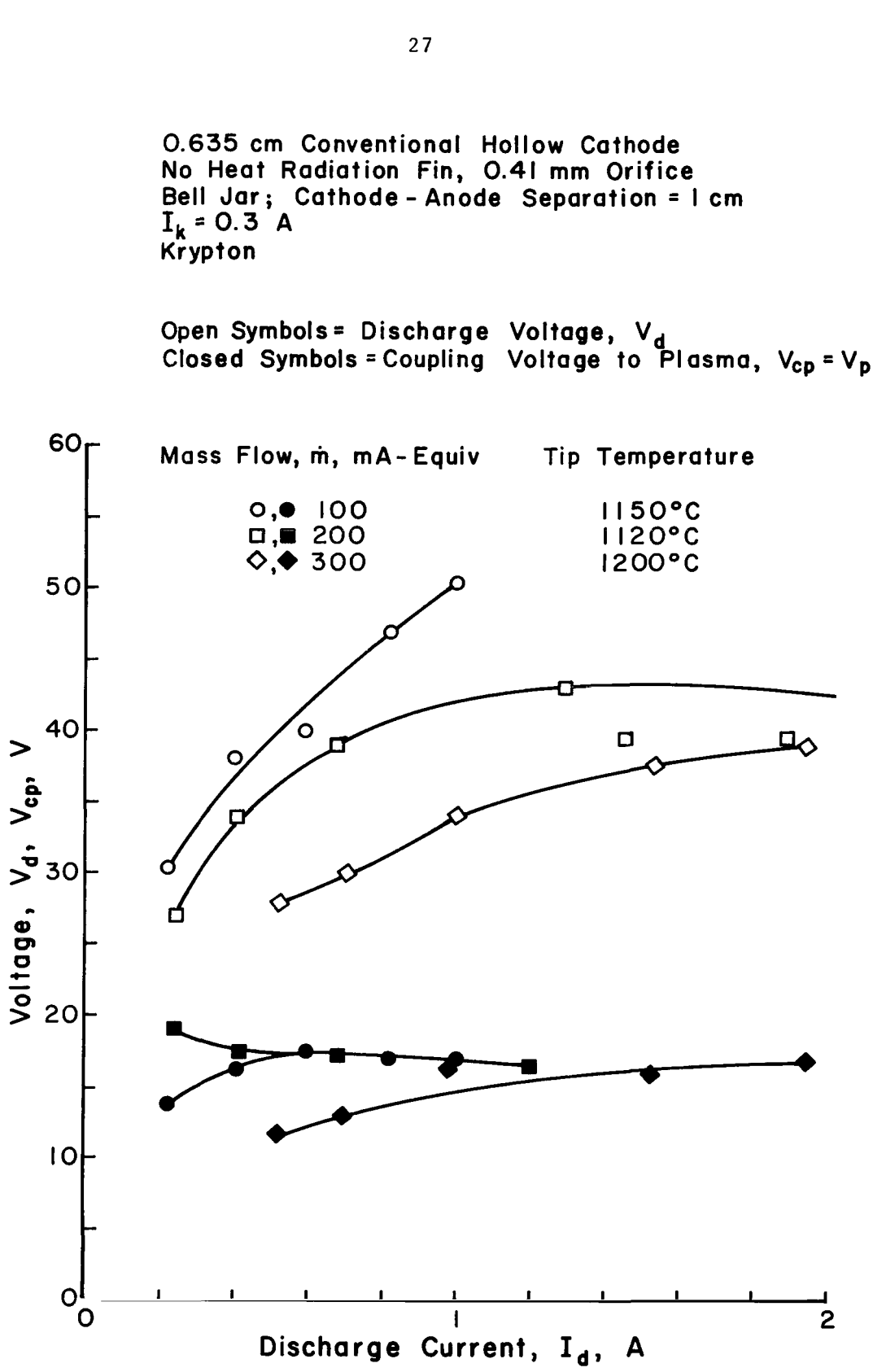

Figure 2-15. Comparison of anode coupling voltage with plasma coupling voltage. Disk anode configuration in bell jar with krypton propellant.

voltage is defined by a Langmuir probe midway between the anode and cathode.) Further, the curve shapes for the two coupling voltages are clearly different. The curves for anode coupling voltage are similar to those obtained with argon (Fig. 2-7). The curves for plasma coupling voltage, though, show the extended horizontal shapes more characteristic of neutralizer operation. The small increase in plasma coupling voltage for the 200 mA-equivalent curve at small discharge currents is not believed to be significant, inasmuch as it is within the accuracy of plasma probe data.

The plasma coupling voltages for bell-jar and neutralizer operation are compared in Fig. 2-16. The difference between the two is substantial at 100 mA-equivalent, and can probably be explained as the difference between spot and plume mode. That is, small differences in configuration parameters are known to change the mode when operation is close to the transition between the two modes. As a specific example, the tip temperatures were significantly higher in the bell jar than when operated as a neutralizer. The curves for the higher propellant flow rates are quite similar, with the major difference only in voltage level. The plasma potential in an ion beam often varies by 10 or 20 volts,[7] so that the difference between the two curves could possibly be explained in terms of the potential difference between the neutralizer location and the center of the ion beam. It would therefore be expected that the agreement between bell jar and neutralizer operation shown in Fig. 2-16 would be much closer if the neutralizer plasma potential were measured close to the neutralizer instead of in the center of the ion beam.

Operating Mode and Electron Emission

Inasmuch as hollow cathodes have been extensively tested with mercury propellant, the information obtained with mercury should serve as a guide in the interpretation of inert-gas test results. Hollow cathode tests with

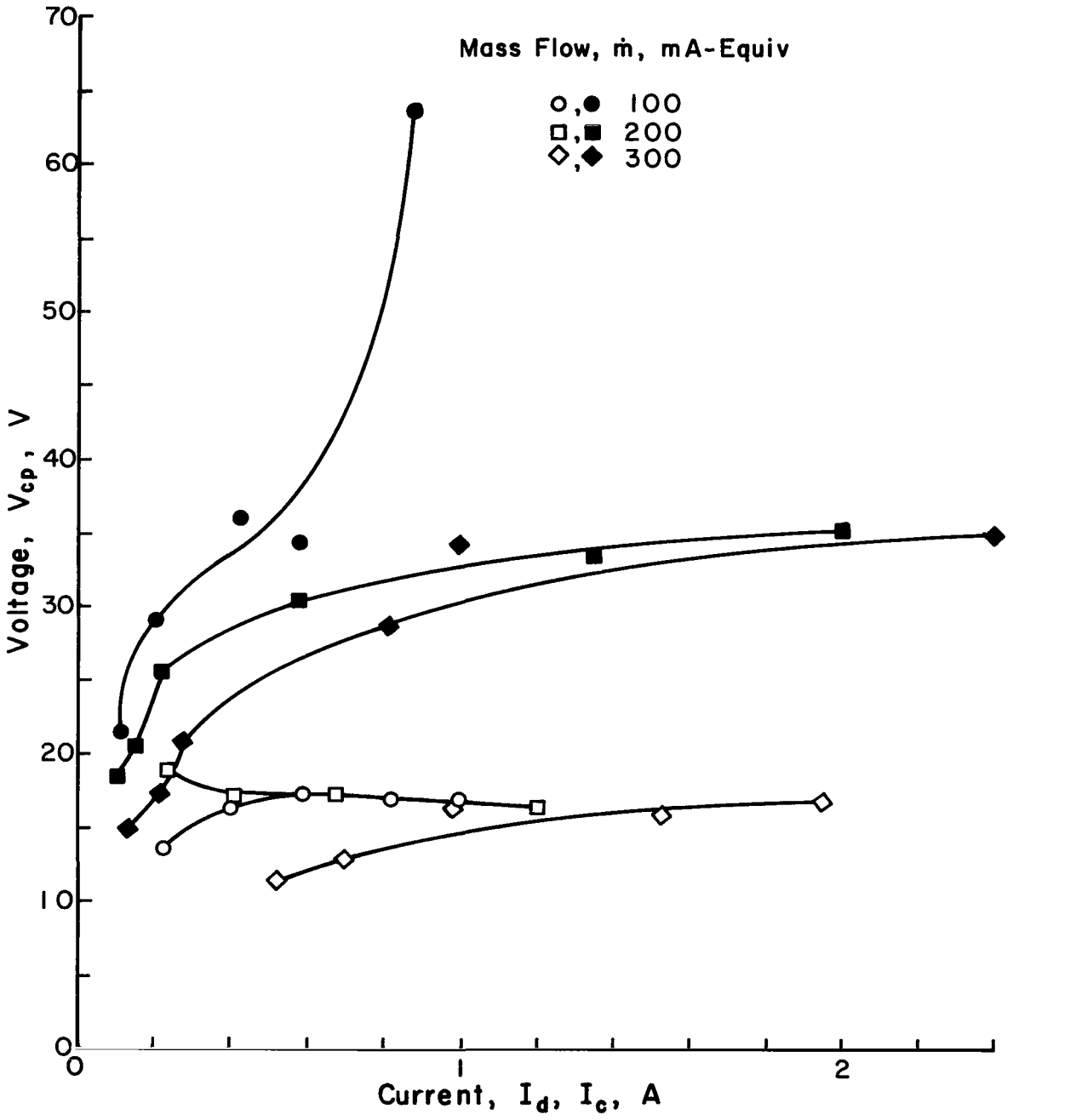

Figure 2-16. Comparison of plasma coupling voltages for bell jar and neutralizer configurations. Krypton propellant.

mercury propellant show at least two distinct modes of operation.[8,9] For high propellant flow rates, small anode-cathode separations, and high electron emissions the spot mode is obtained. Low stable coupling voltages and an intense plasma glow, or spot, near the orifice are the electrical and visual indications of this mode. For low propellant flow rates, large anode-cathode distances, and low electron emissions the plume mode is obtained. High coupling voltages, often fluctuating, and a glowing plume downstream of the orifice (in addition to the glowing spot at the orifice) are the indications of the plume mode. An intermediate transition mode has also been observed with metallic anodes. In this mode the voltage fluctuations can be large and the plume is visible only near the anode. Some of the operating characteristics with spot and plume modes are indicated in Fig. 2-17, which is reproduced from Csiky.[9]

More recent plasma measurements by Wilbur[10] support the viewpoint that the differences between spot and plume modes are associated primarily with changes in the plume region. For either mode, the average Debye length in the vicinity of the orifice is within a factor of several of 10^{-3} mm. The orifice diameter is thus equivalent to many Debye lengths and the plasma should easily penetrate the orifice in either mode. The electron density in the plume region averaged about a factor of 10 lower than the spot mode, while the plasma potential downstream of the orifice was larger by several volts in the plume mode. It appears that the ions required to neutralize the electron space charge come from the orifice in the spot mode. This interpretation is supported by the lack of glow, the high electron density, and the more uniform plasma potential in the plume region for the spot mode. For the plume mode, the charge-neutralization ions appear to be generated within the plume region. The glowing plume and higher overall voltages and electron

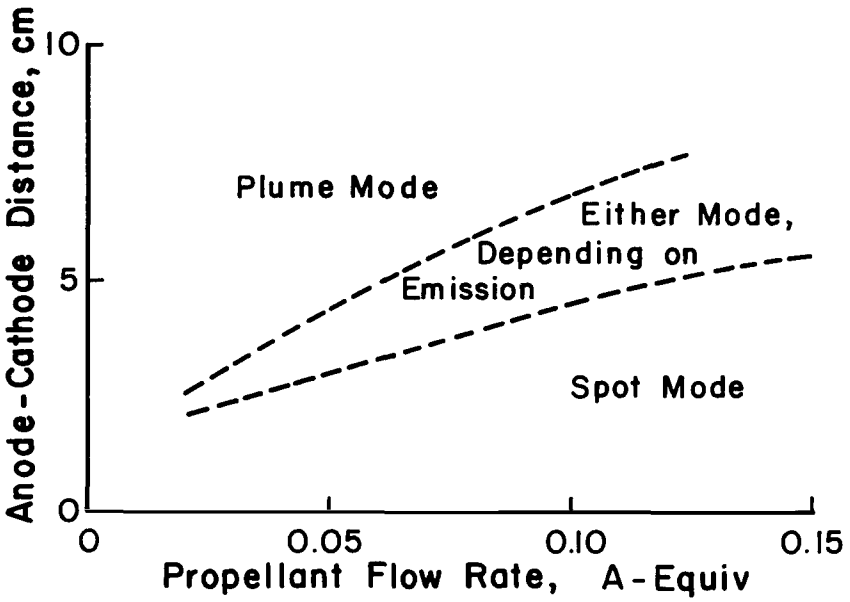

(a) Effect of anode-cathode distance and propellant flow rate on operating mode.

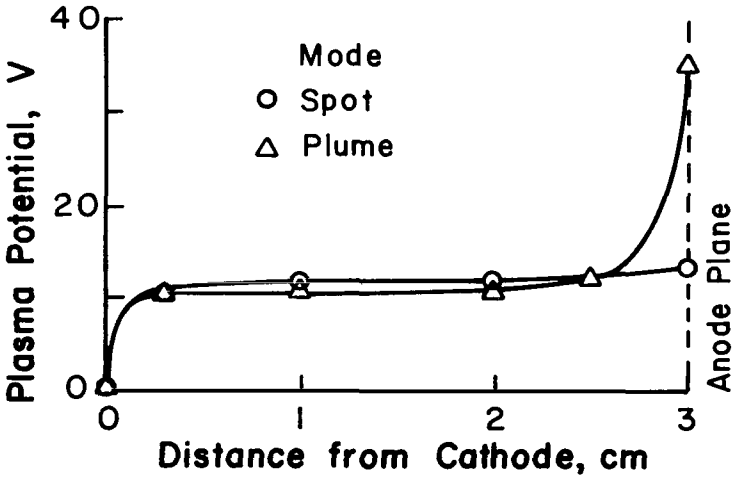

(b) Variation of plasma potential within hollow cathode efflux.

Figure 2-17. Characteristics of spot and plume modes of operation with mercury propellant.

energies support this viewpoint. Also, the more adverse electric fields downstream of the orifice would tend to prevent ions from leaving the orifice and entering the plume region. In the spot mode, then, the charge-neutralizing ions are perhaps carried from the orifice to the plume region by the collisions with neutral atoms or molecules. In the plume mode, plasma mechanisms involving energetic electrons produce these ions within the plume region. It also appears (from both Wilbur's and previous experiments by others) that the plume glow tends to originate near a metallic anode and progresses upstream towards the orifice with increasing departures from spot mode conditions. The upward-turned anode sheath (Fig. 2-17(b)) is an obvious plume-mode mechanism for generating ions. The electrons are accelerated as they approach the anode, typically reaching ionization energy at the equilibrium condition of ion generation. This anode mechanism has been studied in gas discharges and is described by Cobine.[11]

The electron emission from a mercury hollow cathode appears to be due only in part to the thermionic emission from the oxide coated or impregnated insert. This conclusion is supported by test results obtained by Wilbur.[12] Using a calibrated thermionic emitter inside an otherwise conventional hollow cathode, the total cathode emission was two or three times the emitter emission. This result, together with the intense glow in the orifice, clearly indicates that the insert emission is augmented by a discharge mechanism within the orifice. A study by Bessling[13] offers a combination of high field and thermionic emission within the orifice as an additional source of electron emission. Further, this emission within the orifice is localized at surface irregularities, with the intensity of the currents sufficient to cause localized melting in some cases. To complete the picture, the emitted electrons also produce electron-ion pairs within the orifice volume. The

ions that recombine on the orifice walls correspond to an additional emission of electrons.

To the extent that measurements and observations have been made with inert-gas hollow cathodes, they have generally been in agreement with the preceding summary for mercury propellant. One aspect where the agreement has been less clear is the plume luminosity. In going from spot to plume mode with argon, with the mode indicated by electrical measurements, no large change was observed in plume luminosity. The usual appearance with argon was a visible (but not bright) plume, regardless of mode. Fewer observations were made with krypton, but there were similar difficulties in determining the operating mode from plume luminosity with that propellant.

Another area of possible disagreement involves plasma potential measurements. Measurements by Csiky, Fig. 2-17(b), showed that spot-mode plasma potential was close to the anode potential for some distance upstream of the anode. For the plume mode, the upturned sheath near the anode was more typical. For inert-gas operation, however, the upturned sheath at the anode was typical of all operation in which probe measurements were made (see Fig. 2-15). There have not been enough plasma potential measurements for either mercury or inert gases to draw firm conclusions, but it appears that this sheath effect may be the cause of the high coupling voltages with inert gases and a disk anode. As described by Cobine,[11] this upturned sheath is enhanced by reducing anode area. Larger anode areas may therefore reduce this effect and permit better simulation of thruster operation.

A possibly related phenomenon is the adsorption of mercury on surfaces below about 300°C.[14] These adsorbed layers may offset a small anode size when mercury propellant is used with a disk anode. Inert gases are not adsorbed on surfaces at normal operating temperatures,[15] so could not offset

an area effect in a similar manner. More complete plasma measurements will clearly be required to resolve this apparent discrepancy between mercury and inert-gas propellants.

SEM Photographs

Photographs were taken with a scanning electron microscope (SEM) both before and after testing a new cathode with krypton propellant. The specific results have limited interest because of the propellant, but the technique of using SEM photographs of hollow cathodes has important implications for future work.

A 0.61 mm orifice was drilled in the thoriated tungsten tip of a 0.635 cm conventional hollow cathode with a number 73 carbide bit. The photographs shown in Fig. 2-18 were taken before the cathode had been tested, while those in Fig. 2-19 were taken after 3¼ hours of operation at nearly constant conditions. The average operating parameters were at a tip temperature of 950°C, a propellant flow rate of 300 mA-equivalent, a coupling voltage to the disk anode of 35 V, and a coupling voltage to the plasma of 18 V.

Figure 2-18(a) is reproduced herein at a magnification of about 108. Metal flakes from the drilling can be seen along the edge of the orifice. The area between the vertical lines in Fig. 2-18(a) is reproduced in Fig. 2-18(b) at a higher magnification, and a portion of the latter is reproduced at a still higher magnification in Fig. 2-18(c). (Note that the sample was rotated between Figs. 2-18(a) and (b).) The large artifact inside the orifice (assumed to be a tungsten chip) is about 28 microns long. The surface scratches are 1 to 2 microns wide.

Figure 2-19(a) shows the entire cathode orifice after testing. An enlargement of the "8 o'clock" portion of the orifice in Fig. 2-19(a) is

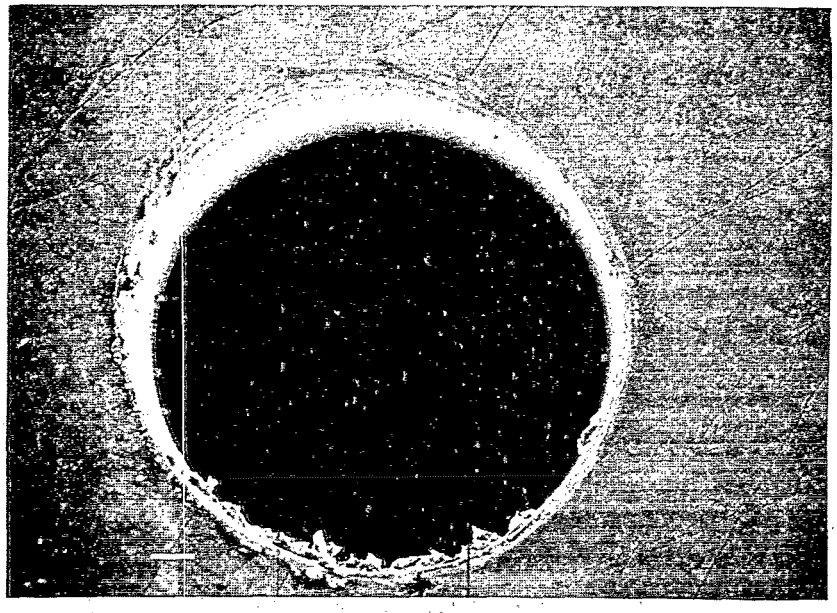

(a) Magnification 108

(b) Magnification 300

Figure 2-18. Cathode orifice before operation.

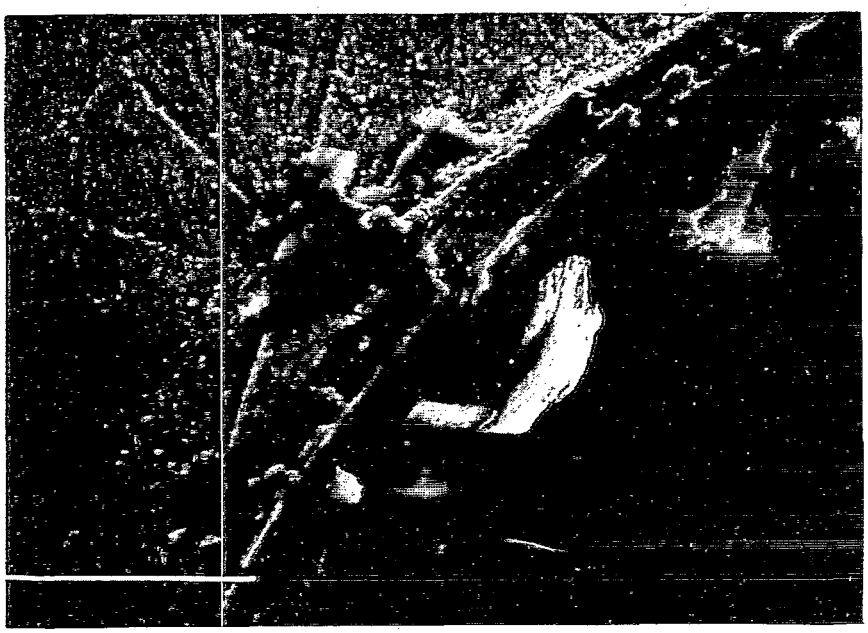

(c) Magnification 700

Figure 2-18. Concluded.

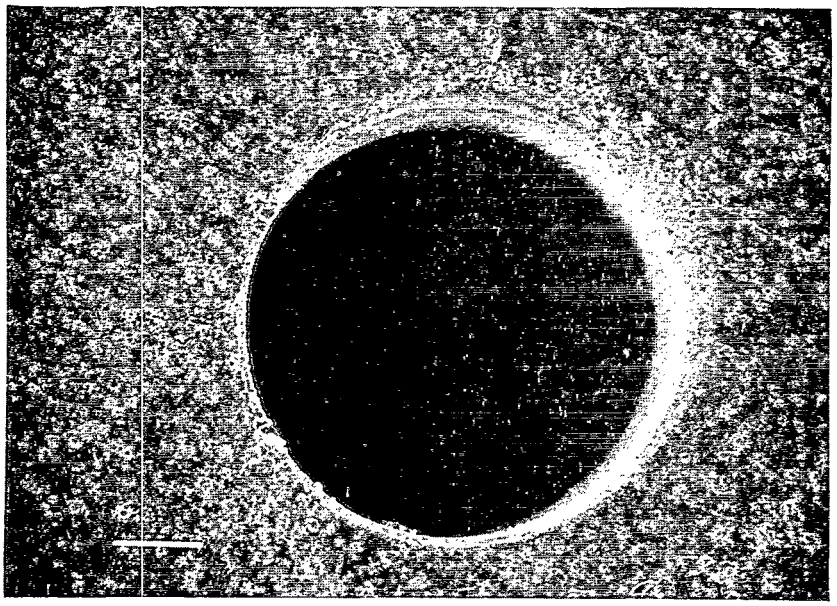

(a) Magnification 96

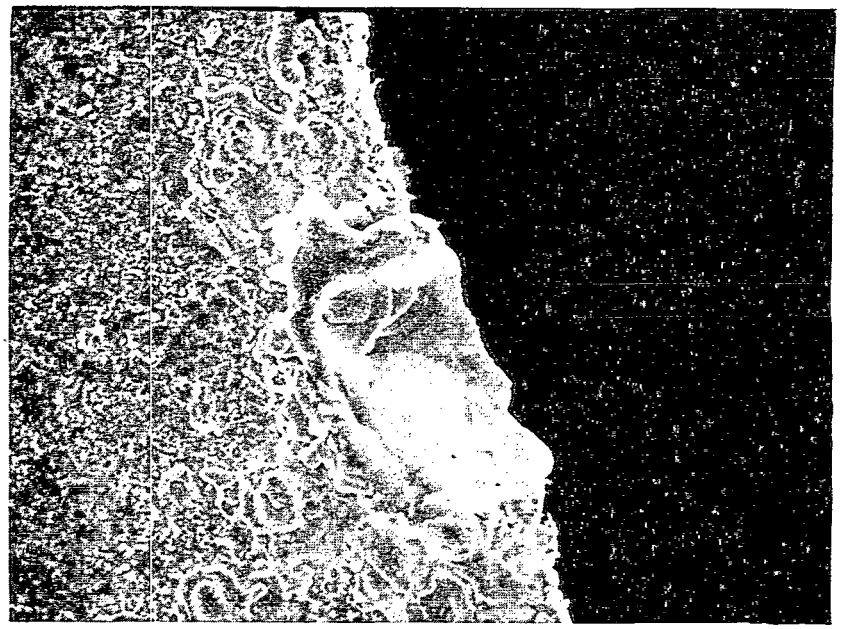

(b) Magnification 960

Figure 2-19. Cathode orifice after operation.

(c) Magnification 3360. Left edge adjoins right edge of photo (d).

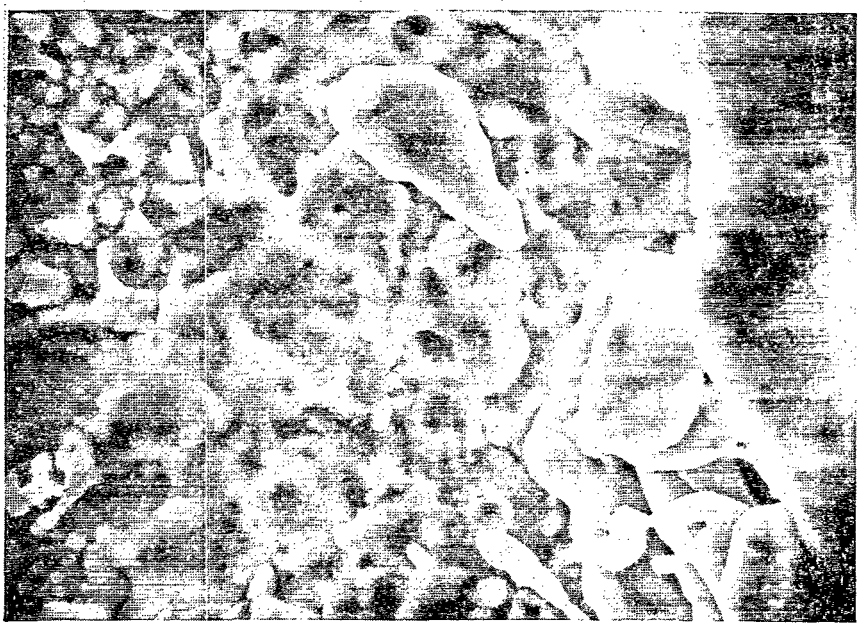

(d) Magnification 4800. Right edge adjoins the left edge of photo (c).

Figure 2-19. Concluded.

shown in Fig. 2-19(b). This latter photograph covers about the same area as Fig. 2-18(b). (Both Fig. 2-18(b) and Fig. 2-19(b) are about 180 degrees from the backwards "N," which is visible in both Fig. 2-18(a) and Fig. 2-19(a).) The artifact of Fig. 2-18(b) has clearly been restructured and only extends some 6 microns into the orifice after testing. Most of the fine surface scratches have also disappeared. Figure 2-19(c) shows the same artifact at a higher magnification, while Fig. 2-19(d) shows the area to the left of Fig. 2-19(c) at a slightly higher magnification. The smallest round shapes shown in Fig. 2-19(d) are 2000 to 4000 Å in diameter.

The restructuring of the artifact shown in Figs. 2-18(b) and 2-19(b) appears to be the result of melting. That is, the observed changes are consistent with melted material flowing under the forces of surface tension. Some of the melted material possibly has spattered or splashed onto the surrounding area (Fig. 2-19(d)). This spattering, if it took place, was probably the result of included elements or compounds flashing to vapor when the tungsten melted. The melting supports Bessling's theory of localized intense currents and heating.[13] The large area-to-volume ratio for the original shape (Fig. 2-18(b)) was conducive to melting. As indicated by Bessling, calculated temperatures are marginal for thoriated tungsten (with mercury propellant), so may only be observed with large area-to-volume ratios. It appears highly likely from the SEM photographs, then, that localized orifice temperatures can greatly exceed the average tip temperature. It also appears likely that these high localized temperatures are involved in electron emission.

Additional SEM photographs (not shown) were taken of the orifice region at various angles. The great depth of field possible with the SEM permits such photographs to be used to construct an accurate profile of the downstream end of the orifice, where most of the wear takes place. This technique should permit estimates of cathode lifetime from runs of only a few tens of hours.

HOLLOW CATHODE PERFORMANCE CORRELATION

The past development of hollow cathodes has been accomplished with mostly trial-and-error methods. Better understanding of hollow cathode operation would hopefully permit a more systematic approach to the development of a new design. One approach to organizing available data is to correlate the performance with suitable parameters. Progress using this approach is described in this section.

One parameter of apparent significance is the ratio of orifice diameter to a mean free path, d/ℓ. To obtain an expression for this parameter, one can start with the flow rate of neutrals.

$$J_o \propto n_o \bar{v}_o A q \propto n_o d^2 (T/W)^{\frac{1}{2}} \qquad (2\text{-}1)$$

Here J_o is the equivalent neutral current, n_o is the neutral density, $\bar{v}_o$ is the average neutral velocity, A is the effective orifice exit area, q is the electronic charge, d is the orifice diameter, T is the neutral temperature, and W is the neutral atomic weight. (A more thorough development of neutral flow through an orifice is given by Rehn.[16]) The neutral temperature is assumed to be nearly a constant for all cathodes. The justification for this assumption comes from the nearly constant tip temperatures that are used, together with the thrust observations of Snyder and Banks.[17] Snyder and Banks measured the thrust of a hollow cathode with and without a discharge at the same propellant flow rate and the same tip temperature. The thrust typically increased by only 28 percent with a discharge, indicating a neutral temperature increase of 64 percent. Despite the high localized temperatures of Bessling, then, the average neutral temperature appears to be approximately governed by the tip temperature. With temperature a constant, solving expression (2-1) for neutral density gives

$$n_o \propto J_o W^{1/2}/d^2. \tag{2-2}$$

The mean free path is

$$\ell \simeq 1/n_o\sigma \propto d^2/J_o W^{1/2}\sigma , \tag{2-3}$$

where σ is the cross section for the pertinent collision process. The desired expression for d/ℓ can therefore be written as

$$d/\ell \propto J_o W^{1/2}\sigma/d \tag{2-4}$$

The parameter $J_o W^{1/2}\sigma/d$ is related to the simpler parameter J_o/d used by Kaufman to correlate spot-plume transitions with mercury propellant.[18] For a single propellant, both W and σ can be assumed to be constants, hence $J_o W^{1/2}\sigma/d$ reduces to J_o/d.

The collision parameter $J_o W^{1/2}\sigma/d$ can be interpreted in at least two ways, depending on the cross section used. If the cross section for electrons to ionize neutrals is used, then the parameter indicates the probability of ion production by electrons emitted in the orifice. If the ion-neutral collision cross section is used, then the parameter indicates the probability of ions being carried out the orifice with the neutral gas. Inasmuch as the different cross sections are nearly proportional for the different inert gases used herein, the particular selection of cross section is probably not important for these gases.

Another parameter of interest is the electron temperature. The overall coupling voltage V would be expected to be roughly proportional to electron temperature and is easier to measure. For the effects of different propellants, the electron temperature should vary as the ionization potential ϕ_i. An appropriate correlation parameter for electron temperature, then is V/ϕ_i .

For a third parameter, we turn to the high-field emission aspect. As discussed in the Operating Mode and Electron Emission section, high electric fields at the wall of the orifice are believed to enhance electron emission from localized hot spots. The localized effects involve local heating, which enhances local electron emission, which increases local ion production and local electric field. The localized effects are not convenient to include in an overall performance parameter, though. A mean value of electric field will therefore be used instead. The electron emission and electron density are related by

$$J_e \propto n_e \bar{v}_e A q \propto n_e d^2 \phi_i^{1/2} \quad . \tag{2-5}$$

Solving for electron density, we find

$$n_e \propto J_e / d^2 \phi_i^{1/2} \quad . \tag{2-6}$$

The Debye length is

$$\ell_D \propto (T_e / n_e)^{1/2} \propto (\phi_i / n_e)^{1/2} \quad . \tag{2-7}$$

With the substitution of electron density,

$$\ell_D \propto \phi_i^{3/4} d / J_e^{1/2} \quad . \tag{2-8}$$

The electric field is a voltage (proportional to ϕ_i) divided by a length (proportional to ℓ_D).

$$E \propto J_e^{1/2} \phi_i^{1/4} / d \tag{2-9}$$

To obtain the first power of emission current J_e, expression (2-9) is squared.

$$E^2 \propto J_e \phi_i^{1/2} / d^2 \tag{2-10}$$

The square of the electric field at the orifice wall should thus be proportional to $J_e \phi_i^{1/2} / d^2$.

Hollow cathode performance is typically presented in terms of the propellant flow, the coupling voltage, and the emission. To make the generalized performance plot relate to these usual presentations, $J_o W^{\frac{1}{2}} \sigma/d$ will be called the mass flow parameter, V/ϕ_i will be called the coupling voltage parameter, and $J_e \phi_i^{\frac{1}{2}}/d^2$ will be called the emission parameter.

The coupling voltage parameter is plotted against the emission parameter for different values of mass flow parameter in Fig. 2-20. The current J_e in the emission current parameter includes both coupling current and keeper current. The cross section used in the mass flow parameter was the maximum value for ionization of neutrals by electrons. (The values used were $3 \times 10^{-20} m^2$ for argon, $4.5 \times 10^{-20} m^2$ for krypton, and $5 \times 10^{-20} m^2$ for xenon.) All the data shown were obtained using a conventional hollow cathode as a neutralizer for a 15-cm thruster. The same inert gas was used for both the thruster and neutralizer. Tip temperatures ranged from 1040 to 1140°C. Three propellants were used, with two orifices tested with argon.

The data of Fig. 2-20 splits into two fairly distinct branches at higher coupling voltages. The left and right branches give substantially different emission currents for the same coupling voltage and are assumed to be associated, respectively, with plume and spot modes. It might be assumed that no distinction can be made between the plume and spot modes at low coupling voltages. Visual observations were, as indicated earlier, somewhat ambiguous. Operation at low coupling voltages, however, clearly showed a visible plume. It is tentatively suggested that all of Fig. 2-20 be considered the plume mode, with the exception of the right branch. Such an interpretation is consistent with the definition of the spot mode as operation with a high value of dJ/dV. From Fig. 2-20, the spot mode appears to be

$$dJ/dV \geq J/V \qquad (2\text{-}11)$$

when defined in this manner.

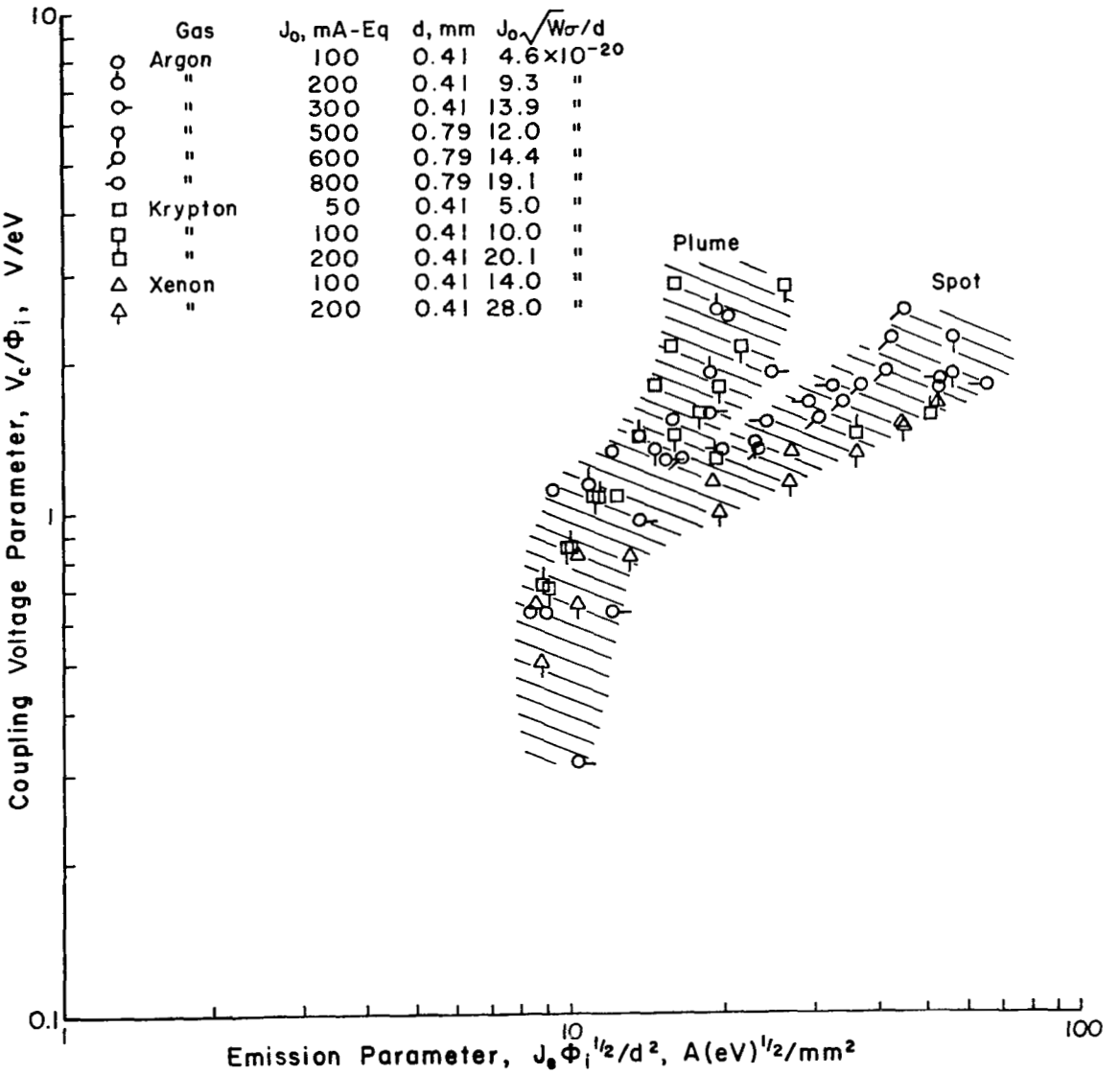

Figure 2-20. Description of hollow cathode performance using the voltage parameter, V_c/ϕ_i, and the emission parameter, $J_e\phi_i^{\frac{1}{2}}/d^2$.

The two branches shown in Fig. 2-20 are associated with different ranges of mass flow parameter. No plume mode data (at high coupling voltages) were obtained above 13.9×10^{-20}. (The units are A-equivalent $(AMU)^{\frac{1}{2}} m^2/mm$.) On the other hand, no spot mode data were observed below 12.0×10^{-20}. The transition range for mercury propellant was 0.14 to 0.40 for J_o/d (A-equivalent/mm). Using a cross section of $5 \times 10^{-20} m^2$ for mercury, the equivalent range in $J_o W^{\frac{1}{2}} \sigma/d$ is 10 to 28×10^{-20}. The mercury propellant data were obtained over a wider range of cathode sizes, tip temperatures, and coupling configurations than the data of Fig. 2-20, so that the wider transition range is not surprising.

The correlation parameters shown in Fig. 2-20 were only three of many that were tried. Several other parameters tried were proportional to the ratio of Debye distance to orifice diameter. The use of this latter ratio is consistent with the earlier viewpoint that transition from plume to spot mode results from the Debye distance becoming small enough for the discharge plasma to penetrate the orifice. Parameters proportional to this ratio, however, did not give any correlation approaching that shown in Fig. 2-20. This lack of correlation, together with the recent plasma property measurements of Wilbur,[10] strongly indicate that the Debye distance is small compared to the orifice diameter in any operating condition normally of interest in electric propulsion.

III - ARGON-XENON DISCHARGE CHAMBER MODEL FOR THE PRODUCTION OF DOUBLY CHARGED IONS THEORY

by Paul J. Wilbur

The ion thruster discharge chamber model developed by Peters[1] has been adapted for use with argon and xenon propellants. In discussing this model argon will be used as an example but the same basic equations and reactions will apply to xenon when such constants as the xenon atomic weight are substituted.

The reactions considered important in this analysis are:

$$Ar + e^- \rightarrow Ar^+ + 2e^-$$

$$Ar + e^- \rightarrow Ar^{++} + 3e^-$$

$$Ar^+ + e^- \rightarrow Ar^{++} + 2e^-$$

and the electrons inducing these reactions are assumed to consist of a Maxwellian group and a monoenergetic or primary group. Once the ionic argon states have been produced, they are assumed to migrate to the boundary of the ion production region where they either recombine with an electron and are returned to the chamber as neutral argon or are extracted from the chamber through the accelerator grids and replaced by atoms from the propellant feed system. Ions migrate at a rate determined by the Bohm criterion for a stable sheath.[2] By equating the production and loss rates of singly charged ions the ratio of neutral atom-to-singly charged ion densities can be determined. The resultant equation is:

$$\frac{n_o}{n_+} = \frac{1}{\Psi/A} \frac{\left[\frac{e}{m_i} T_{mx} (1 + n_{pr}/n_{mx})\right]^{\frac{1}{2}}}{F_+ \left[n_{pr} P_o^+(\xi_{pr}) + n_{mx} Q_o^+ (T_{mx})\right]} \qquad (3\text{-}1)$$

where

n_o = neutral atom density (m^{-3})

n_+ = singly charged ion density (m^{-3})

Ψ/A = volume-to-surface area ratio of the primary electron (ionizing) region (m)

e = electronic charge (1.6×10^{-19} coul).

m_i = ion mass (kg)

T_{mx} = Maxwellian electron temperature (eV)

n_{pr} = Primary electron density (m^{-3})

n_{mx} = Maxwellian electron density (m^{-3})

ξ_{pr} = Primary electron energy (eV)

F_+ = Plasma uniformity factor relating singly charged ion flux at the boundary to that in the body of the ionizing plasma -- See Peters[1] for additional discussion.

$P_o^+ (\xi_{pr})$ = Primary Rate Factor (electron velocity-cross section product) for the neutral-to-singly ionized reaction induced by primary electrons at an energy ξ_{pr}. Figures 3-1 and 3-2 are plots of this quantity for both the argon and xenon reactions.

$Q_o^+ (T_{mx})$ = Maxwellian Rate Factor (electron velocity-cross section product) for the neutral-to-singly ionized reaction calculated over the Maxwellian distribution function for electrons at a temperature T_{mx}. Figures 3-3 and 3-4 are plots of this quantity for the argon and xenon reactions.

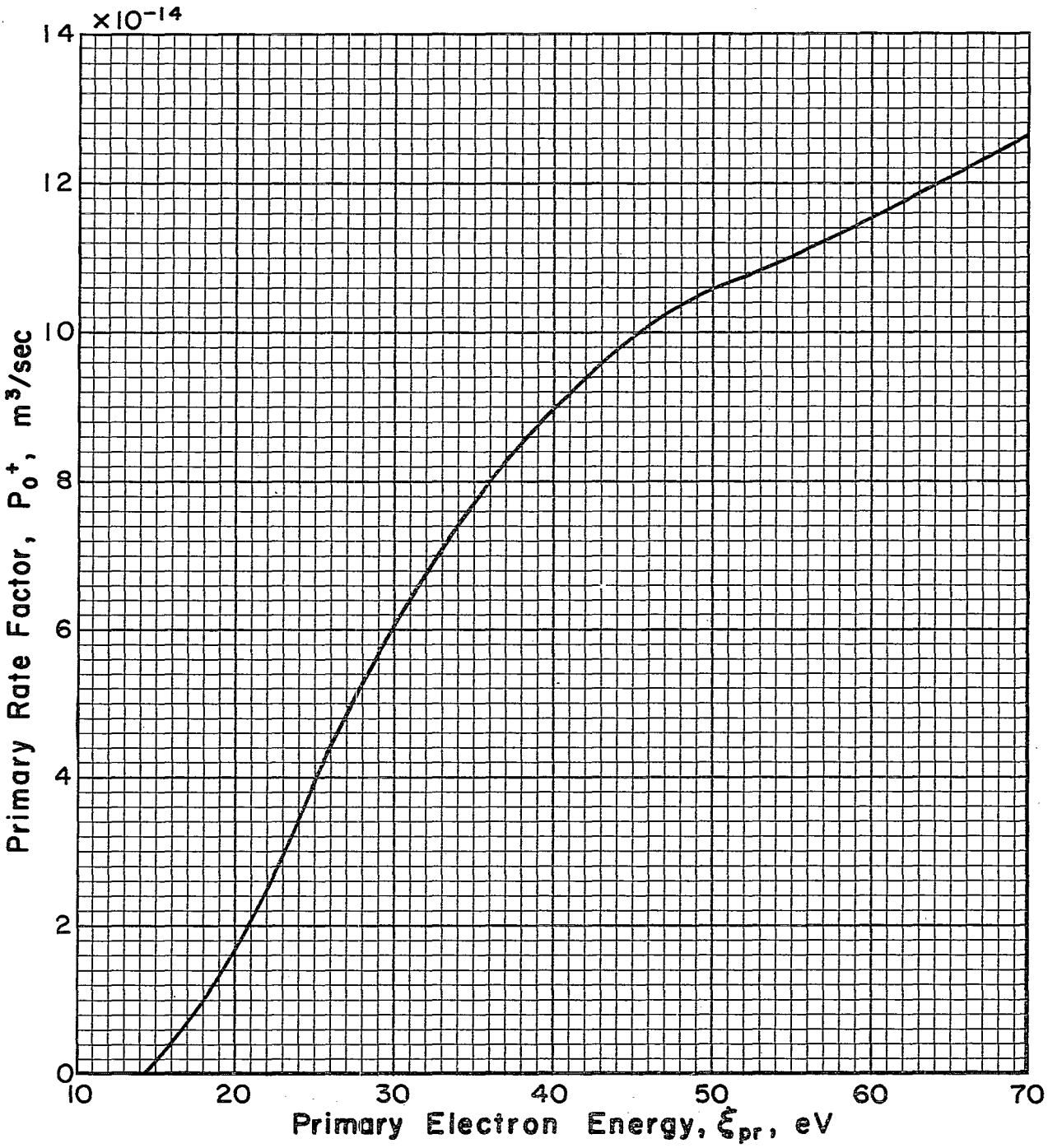

Fig. 3-1: Primary rate factor P_o^+ for argon as a function of primary electron energy.

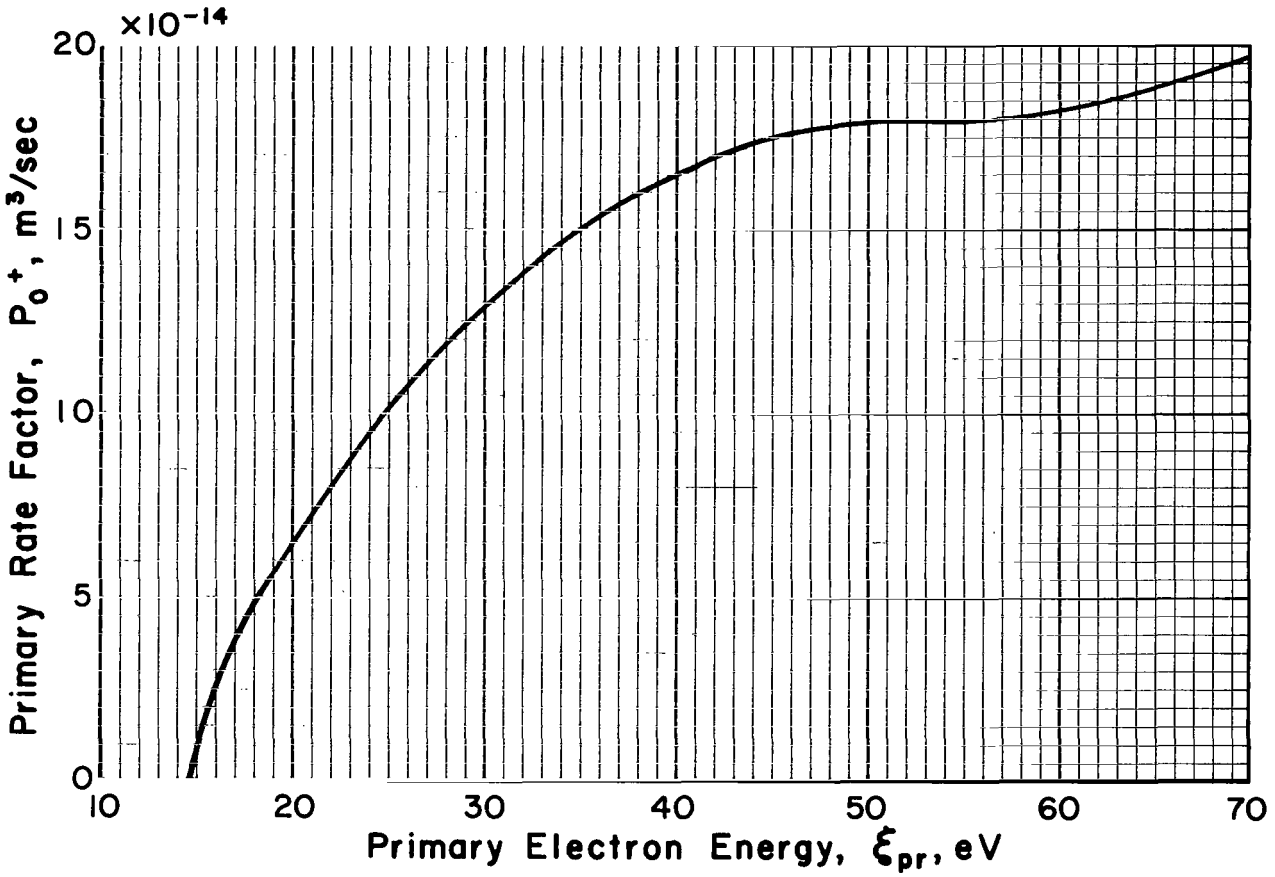

Fig. 3-2: Primary rate factor P_o^+ for xenon as a function of primary electron energy.

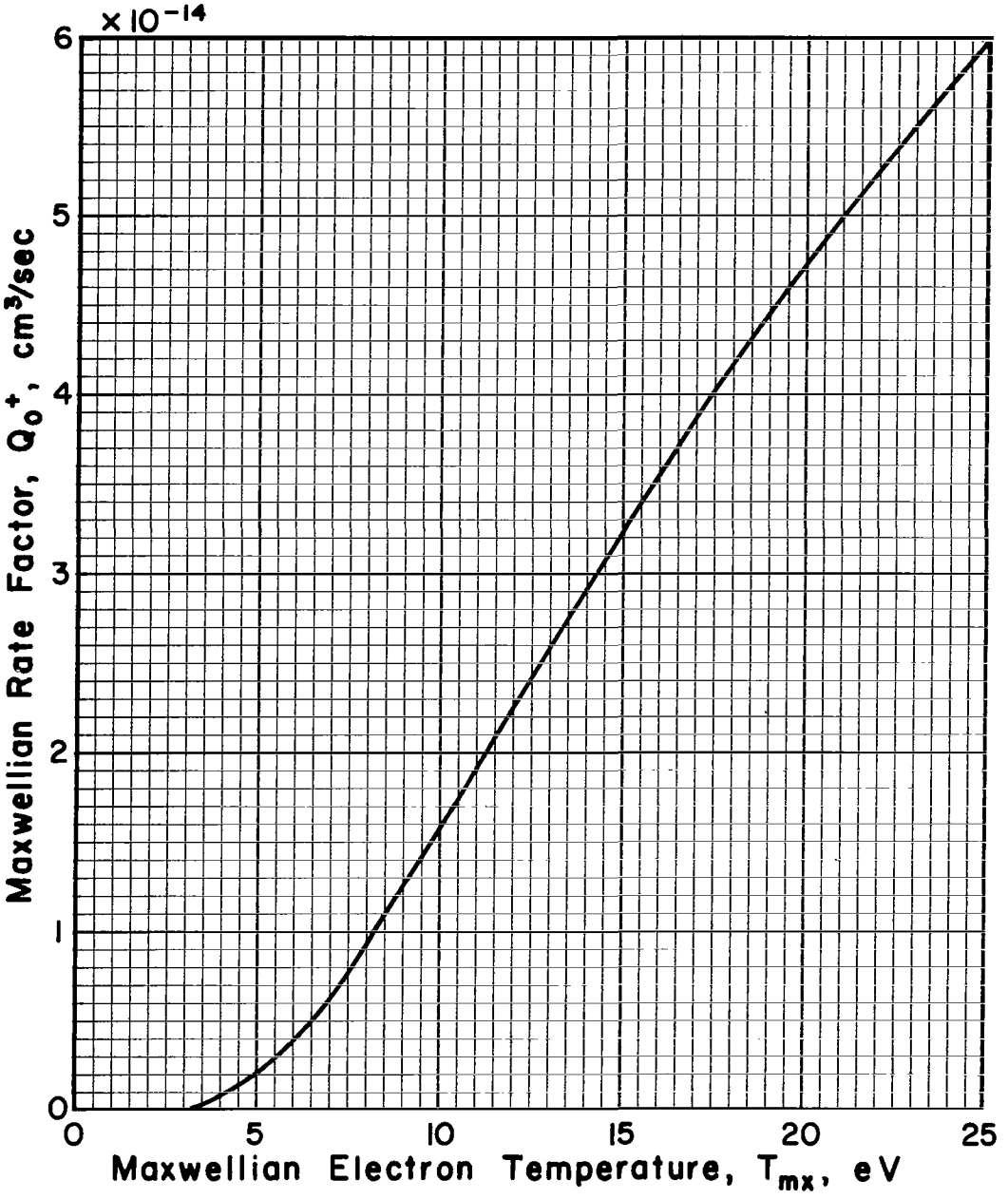

Fig. 3-3: Maxwellian rate factor Q_o^{++} for argon as a function of Maxwellian electron temperature.

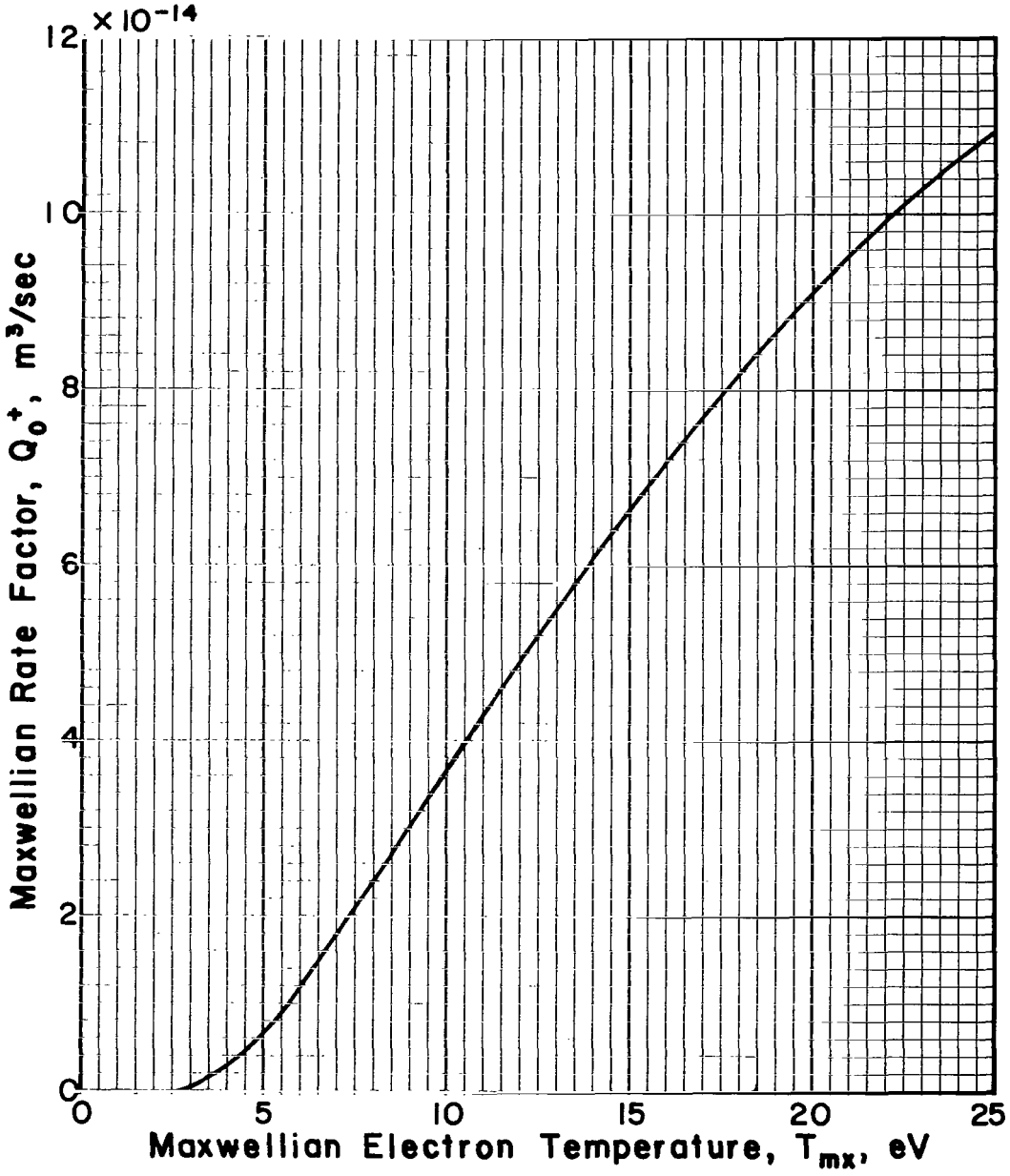

Fig. 3-4: Maxwellian rate factor Q_o^+ for xenon as a function of Maxwellian electron temperature.

Cross sections used to calculate P_o^+ and Q_o^+ and other rate factors used in this analysis have been obtained from Kieffer and Dunn.[3]

When one equates the production and loss relations for doubly charged ions to determine the equilibrium doubly-to-singly charged ion density ratio the following expression is obtained:

$$\frac{n_{++}}{n_+} = \frac{V/A\ F_{++}\ [n_{pr}\ (P_+^{++}\ (\xi_{pr}) + \frac{n_o}{n_+}\ P_o^{++}\ (\xi_{pr})) + n_{mx}\ (Q_+^{++}(T_{mx}) + \frac{n_o}{n_+}\ Q_o^{++}\ (T_{mx}))]}{[2T_{mx}\ \frac{e}{m_i}\ (1 + n_{pr}/n_{mx})]^{\frac{1}{2}}} \qquad (3\text{-}2)$$

Most of the symbols in equation (2) have been defined but the following have not:

F_{++} = Plasma uniformity factor relating doubly charged ion flux at the boundary to that in the body of the ionizing plasma -- See Peters[1] for additional discussion.

$P_+^{++}\ (\xi_{pr})$ = Primary Rate Factor for the singly-to-doubly charged ionizing reaction induced by primary electrons at an energy ξ_{pr}. This quantity is plotted in Figs. 3-5 and 3-6.

$P_o^{++}\ (\xi_{pr})$ = Primary Rate Factor for the neutral-to-doubly charged ionizing reaction induced by primary electrons at an energy ξ_{pr}. This quantity is plotted in Figs. 3-7 and 3-8.

$Q_+^{++}\ (T_{mx})$ = Maxwellian Rate Factor for the singly-to-doubly charged ionizing reaction calculated over the Maxwellian distribution function for electrons at a temperature T_{mx}. This quantity is plotted in Figs. 3-9 and 3-10.

$Q_o^{++}\ (T_{mx})$ = Maxwellian Rate Factor for the neutral-to-doubly charged ionizing reaction calculated over the Maxwellian distribution function for electrons

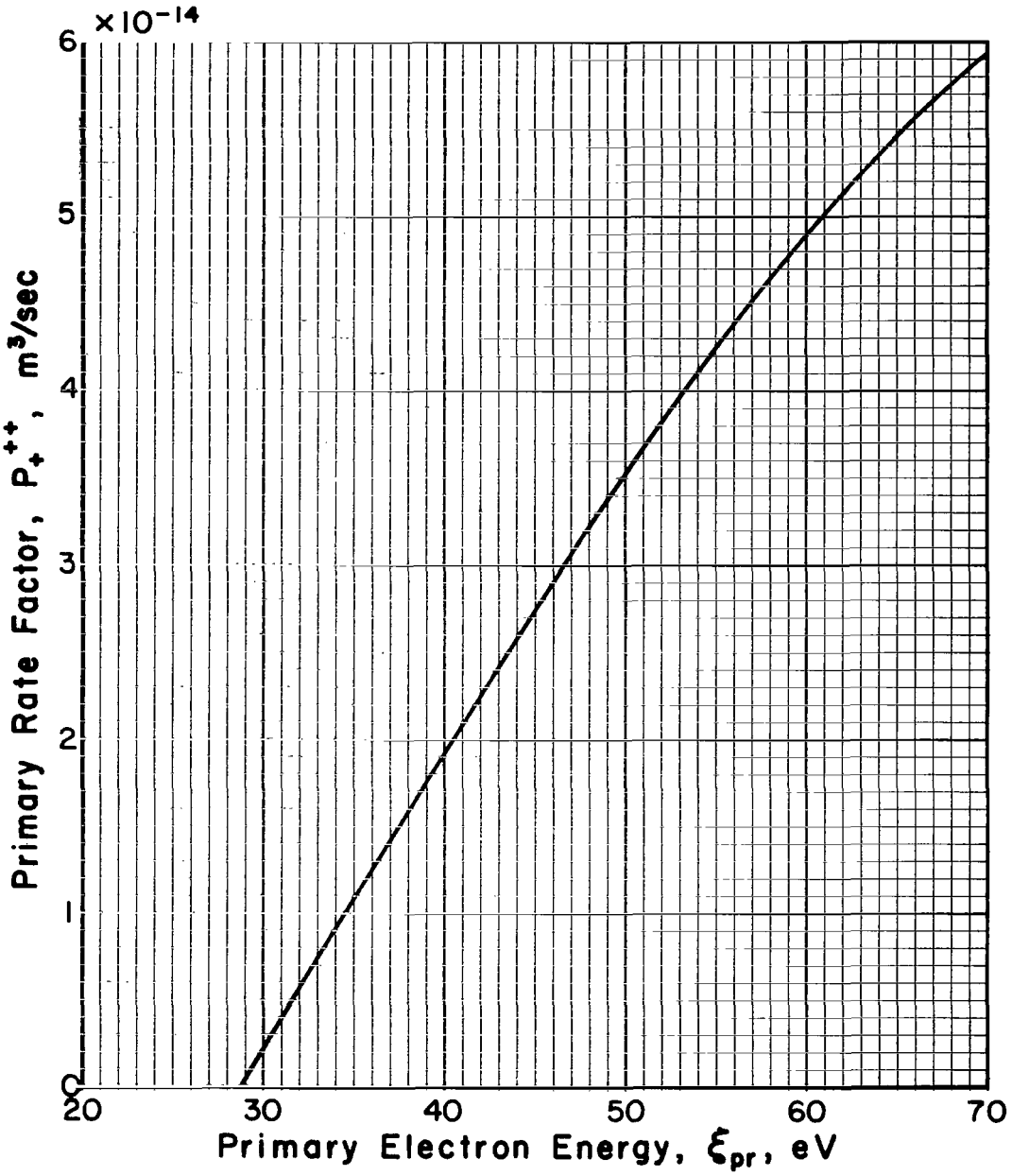

Fig. 3-5: Primary rate factor P_+^{++} for argon as a function of primary electron energy.

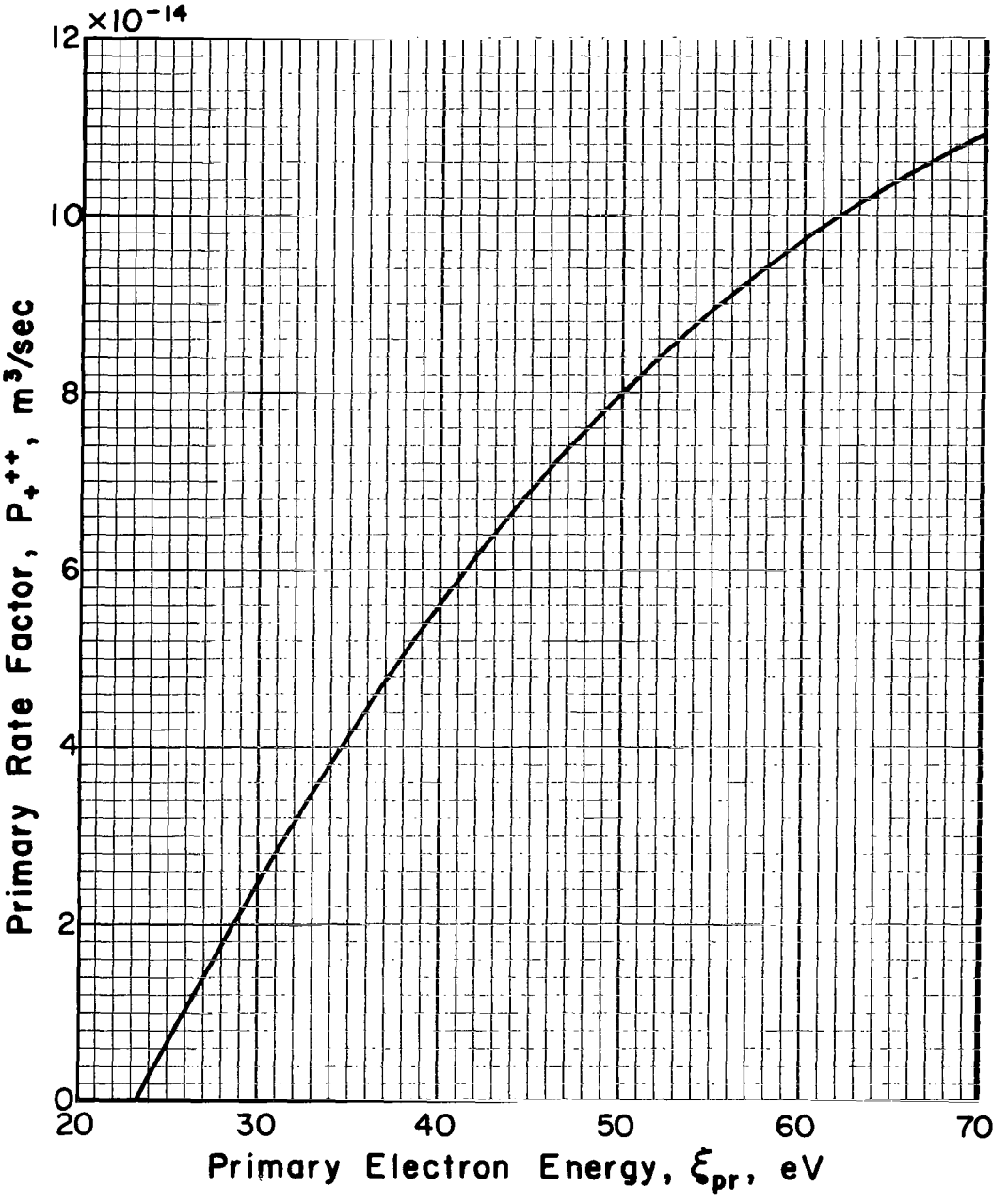

Fig. 3-6: Primary rate factor P_+^{++} for xenon as a function of primary electron energy.

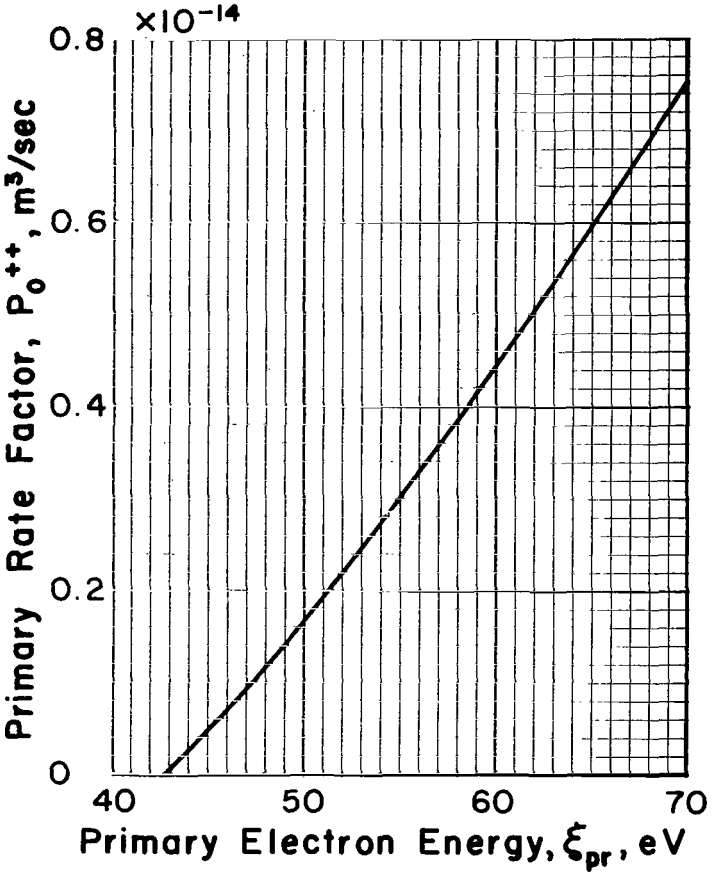

Fig. 3-7: Primary rate factor P_o^{++} for argon as a function of primary electron energy.

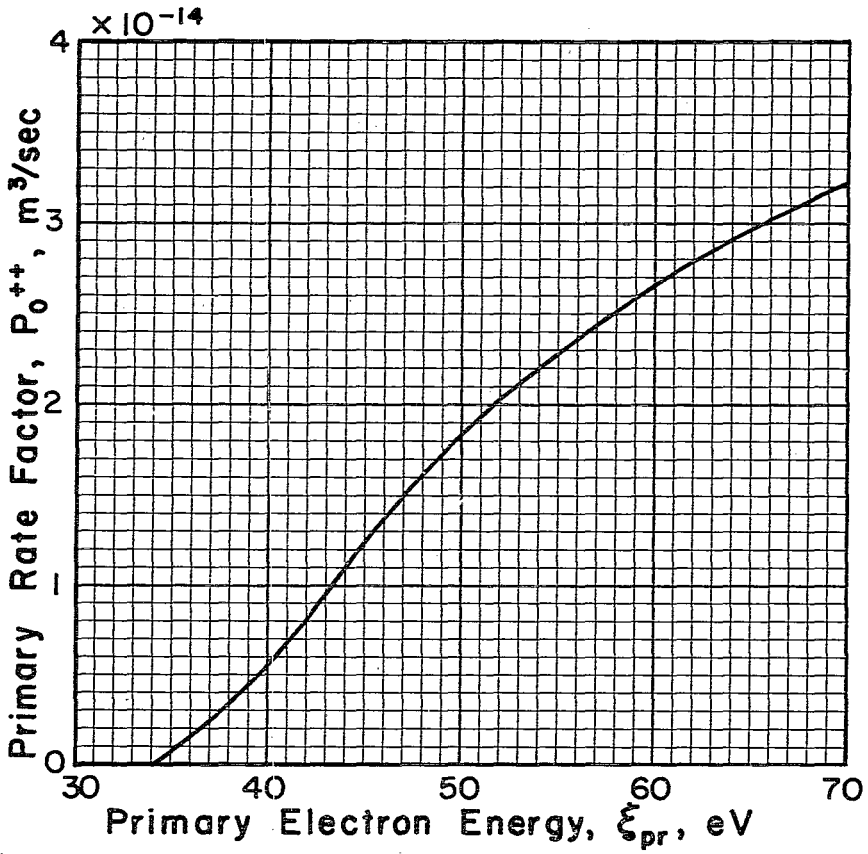

Fig. 3-8: Primary rate factor P_o^{++} for xenon as a function of primary electron energy.

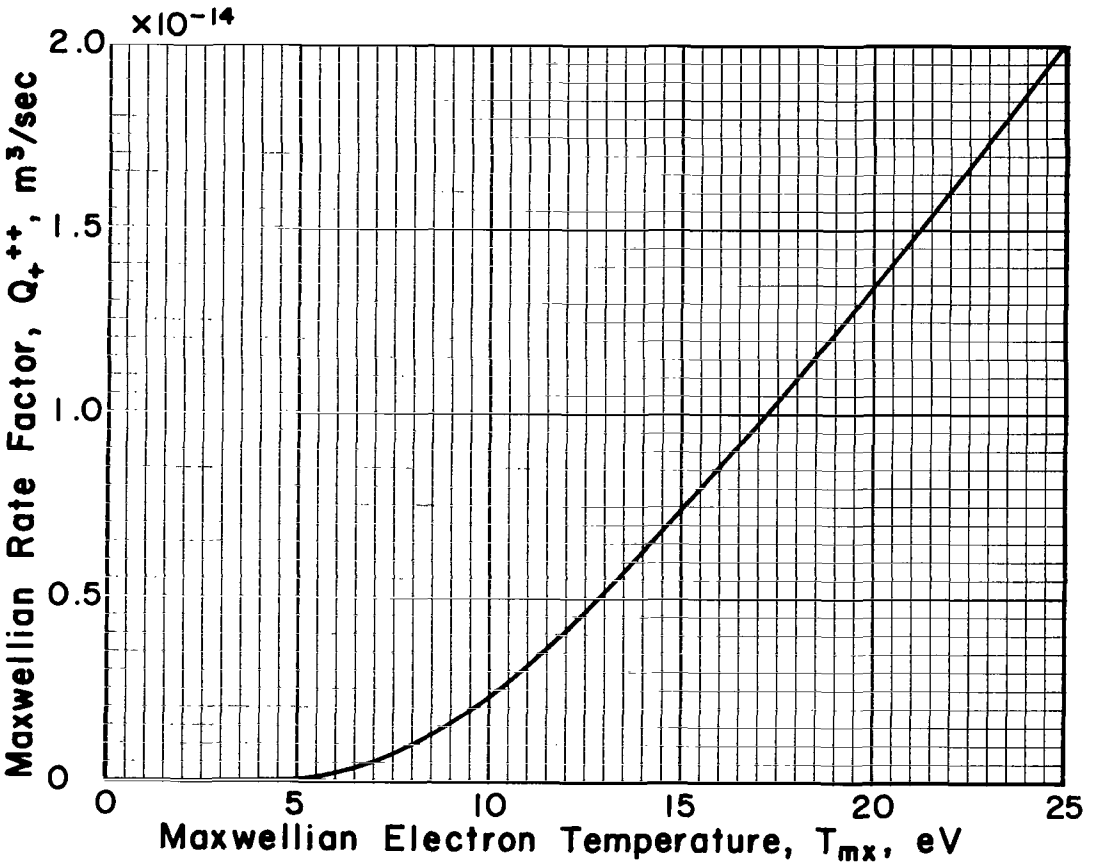

Fig. 3-9: Maxwellian rate factor Q_+^{++} for argon as a function of Maxwellian electron temperature.

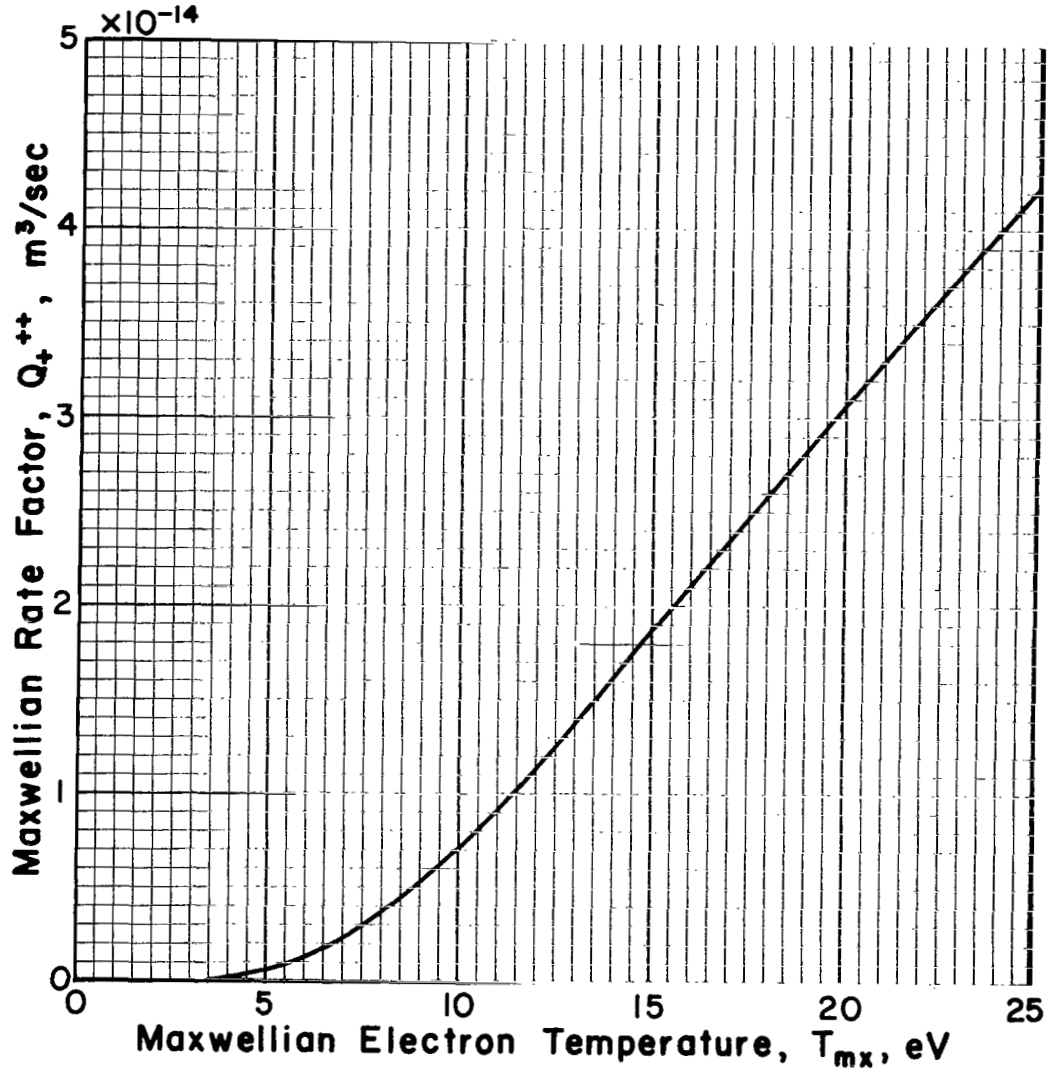

Fig. 3-10: Maxwellian rate factor Q_+^{++} for xenon as a function of Maxwellian electron temperature.

at a temperature T_{mx}. This quantity is plotted in Figs. 3-11 and 3-12.

The data used to construct Figs. 1-12 are also presented in Table 3-1.

MODEL VERIFICATION

Simultaneous measurements made by Isaacson[4] of plasma properties and doubly-to-singly charged ion ratios in a multipole thruster have been used to evaluate the validity of the model proposed. These data were collected over a range of thruster lengths and argon and xenon flow rates in a 15 cm diameter thruster. Plasma properties were obtained using Langmuir probes and doubly-to-singly charged ion densities were determined from doubly-to-singly charged ion current density measurements made in the ion beam using a mass spectrometer.

Figure 3-13 shows the correlation between the measured values of doubly-to-singly charged ion density ratios and those obtained using measured plasma properties in the model discussed herein. Each data point shows the measured and calculated density ratio for a different thruster length or flow rate. The 45° line drawn through the data corresponds to perfect correlation between the results of the model and the measured double-to-singly charged ion density ratios. The data are seen to lie close to the line with all but one point enclosed within the ± 20% error band. The number next to each data point is the number of multipole thruster side sections on the thruster configuration used in the corresponding test. The number four, for example, indicates four side sections were used and since each section is 2.7 cm long this configuration would have had a total length of 10.8 cm.

Doubly-to-singly charged ion density ratios were observed to be much lower with argon than they were with xenon. This can be seen in the data of Figure 3-13. The model shows the reason for this is the smaller argon cross sections and the lower argon mass, both of which appear in the nu-

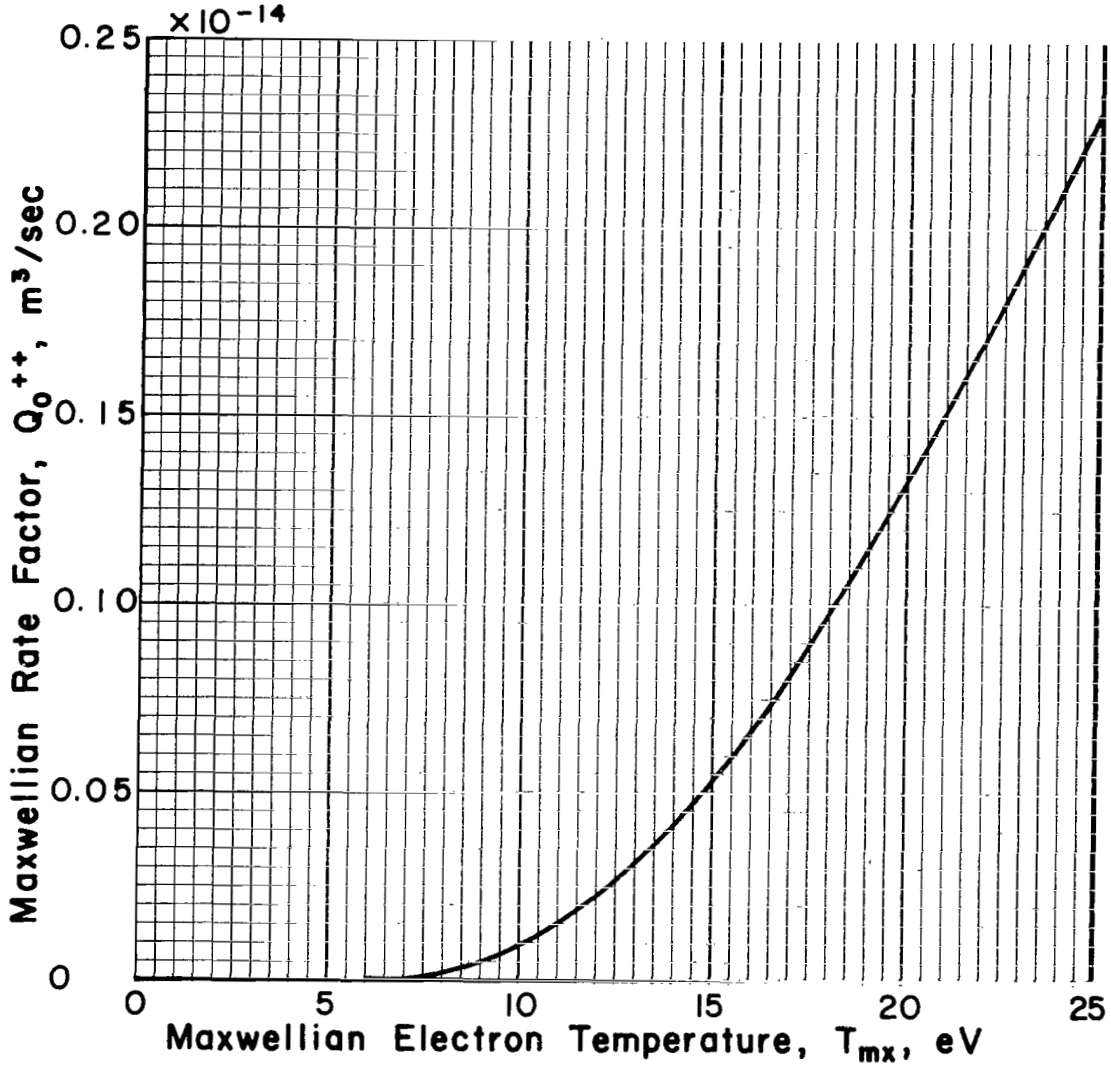

Fig. 3-11: Maxwellian rate factor Q_o^{++} for argon as a function of Maxwellian electron temperature.

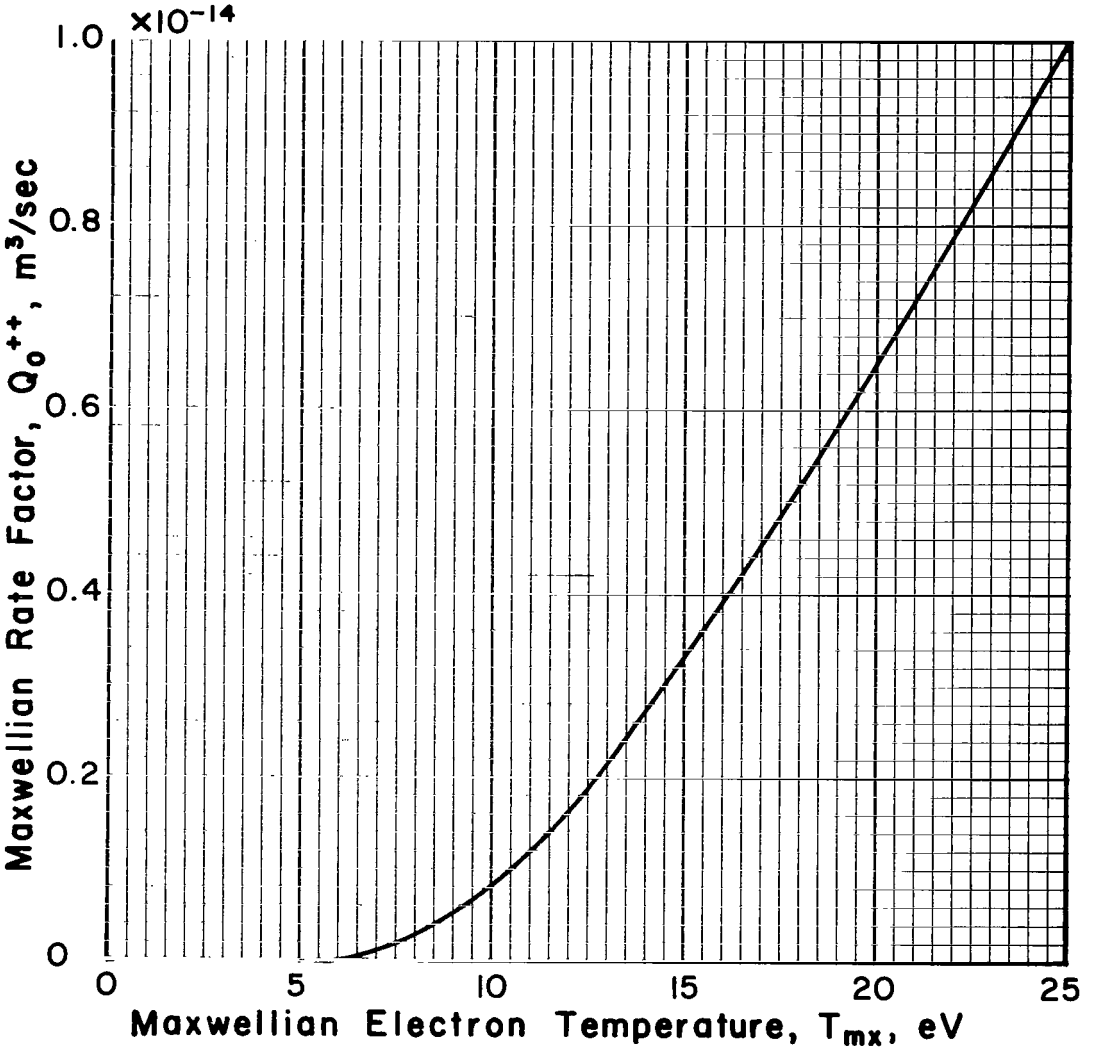

Fig. 3-12: Maxwellian rate factor Q_o^{++} for xenon as a function of Maxwellian electron temperatures.

Table 3-1 - Rate Factors

ARGON

Temp (eV)	Q_o^+ (m^3/sec)	Q_o^{++} (m^3/sec)	Q_+^{++} (m^3/sec)	Energy (eV)	P_o^+ (m^3/sec)	P_o^{++} (m^3/sec)	P_+^{++} (m^3/sec)
3	0.019×10^{-14}	-	0.0001×10^{-14}	5	-	-	-
4	0.086	-	0.002	10	-	-	-
5	0.22	-	0.008	15	0.002×10^{-13}	-	-
6	0.41	0.004×10^{-15}	0.025	20	0.17	-	-
7	0.66	0.012	0.053	25	0.39	-	-
8	0.95	0.029	0.097	30	0.60	-	0.245×10^{-14}
9	1.26	0.057	0.15	35	0.77	-	1.04
10	1.58	0.099	0.23	40	0.89	-	1.90
12	2.25	0.23	0.40	45	0.99	0.05×10^{-14}	2.76
15	3.24	0.55	0.73	50	1.06	0.17	3.55
18	4.15	0.99	1.10	60	1.15	0.44	4.89
21	4.98	1.52	1.49	70	1.26	0.75	5.94
24	5.72	2.10	1.88	80	1.32	1.07	6.73
27	6.38	2.71	2.25	90	1.35	1.32	7.33
30	6.98	3.33	2.61	100	1.33	1.45	7.83

XENON

3	0.009×10^{-13}	-	0.002×10^{-14}	5	-	-	-
4	0.032	0.0003×10^{-14}	0.014	10	-	-	-
5	0.071	0.0018	0.051	15	$.13 \times 10^{-13}$	-	-
6	0.12	0.0063	0.12	20	.63	-	-
7	0.18	0.016	0.23	25	1.00	-	0.071×10^{-13}
8	0.24	0.032	0.37	30	1.29	-	0.25
9	0.31	0.055	0.53	35	1.51	0.065×10^{-14}	0.42
10	0.37	0.085	0.73	40	1.64	0.50	0.57
12	0.50	0.166	1.16	45	1.74	1.27	0.69
15	0.67	0.327	1.89	50	1.79	1.86	0.80
18	0.82	0.517	2.63	60	1.82	2.64	0.97
21	0.95	0.721	3.35	70	1.97	3.20	1.09
24	1.06	0.925	4.02	80	2.10	3.63	1.18
27	1.16	1.13	4.65	90	2.18	3.99	1.24
30	1.25	1.32	5.22	100	2.19	4.36	1.29

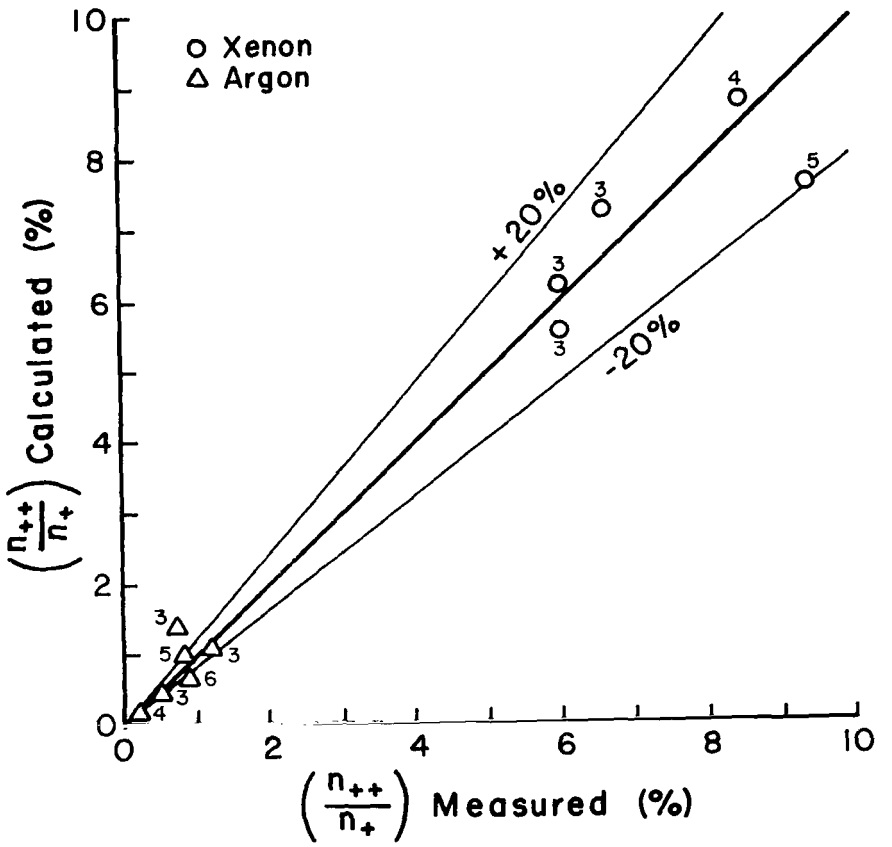

Fig. 3-13: Double-to-single ion density ratio. Correlation between theory and experiment.

merator of equation (3-2).

Consideration of the relative magnitude of each of the terms of Equation (2) shows the relative contribution of each of the processes and ionizing species considered in the analysis. Such an examination reveals that doubly charged ions are produced by both primary and Maxwellian electrons in significant numbers for both argon and xenon. Likewise doubly charged ions are produced by both one (neutral-to-doubly ionized) and two step (neutral-to-singly ionized followed by singly-to-doubly ionized) processes.

CONCLUSION

The model developed by Peters[1] to calculate the ratio of doubly-to-singly charged ions in a mercury discharge chamber can be applied for similar calculations in argon and xenon plasmas. Only neutral, singly ionized and doubly ionized ground state atoms need be considered in the analysis. Double-to-single ion density ratios claculated from average plasma properties in the discharge chamber can be expected to agree with measured values to within ± 20%.

IV - PROPELLANT ISOLATOR

by Raymond S. Robinson

Supplying a propellant to a thruster usually requires electrical isolation between the discharge chamber and the source of the propellant, which is usually at ground (spacecraft) potential. The arrangement of thruster and isolator used in this investigation is shown in Fig. 4-1. Stainless steel tubing with an inside diameter of 1.6 mm was used between the gas supply and the isolator, and between the isolator and the thruster. About 8 cm of tubing were used between the isolator and a manifold, from which four tubes went to the thruster (only two shown in Fig. 4-1). The shortest of these four tubes was about 15 cm, so that the minimum tube length from the isolator to the thruster was about 23 cm. There was an additional several centimeters of path length in the propellant distributor within the thruster.

The isolator configurations tested are shown in Fig. 4-2. Aluminum oxide tubing with an inside diameter of 3.2 mm was used for all the isolator bodies. Configuration I was a simple tube with an insulating length of 7.7 cm. For configuration II, the insulating length was increased to 18.4 cm. The configuration II isolator body was used in configuration III, but two de-ionizing pads of fine steel wool were also used. These pads were about 0.5 cm long and located so that the tube was divided into three equal segments. The propellant was argon.

The test results are shown in Fig. 4-3 for an operating thruster. Breakdowns were observed as current surges of several hundred milliamperes in the beam power supply, together with bright blue or pink glows through the isolator walls. Configurations I and II were single segment isolators, so the breakdown potential difference shown was for the entire isolator. Flows

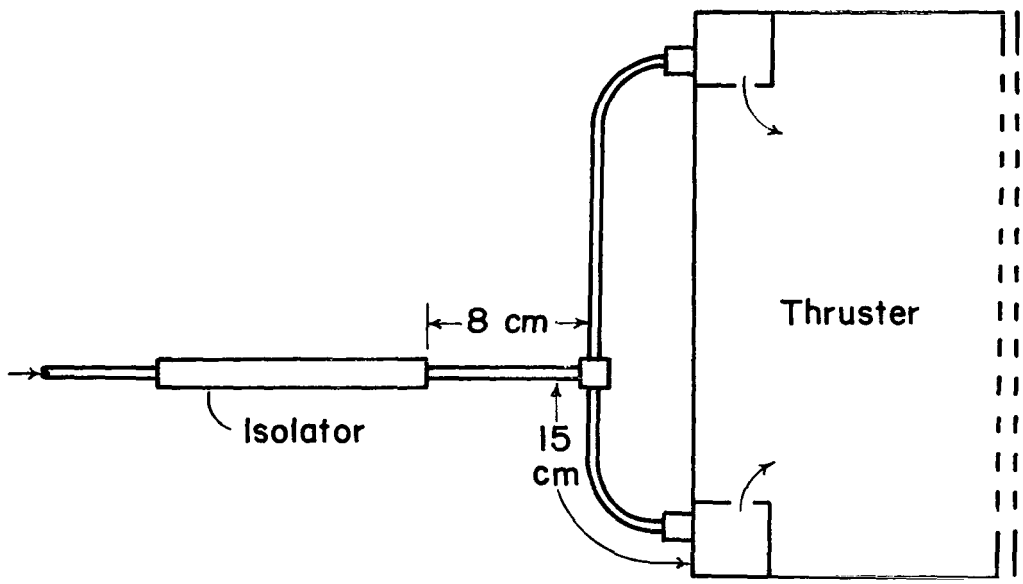

Fig. 4-1: Inert gas propellant feed between isolator and thruster.

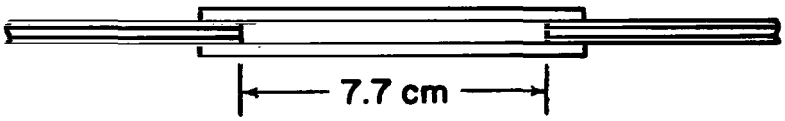

(a) Configuration I

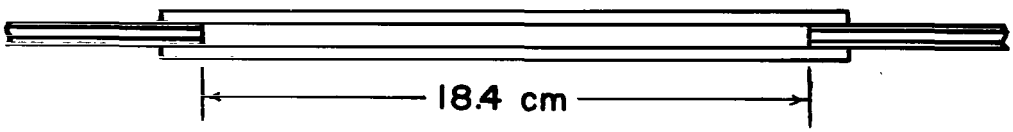

(b) Configuration II

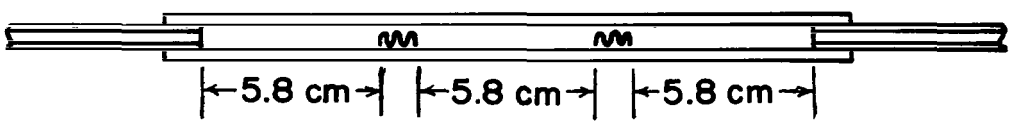

(c) Configuration III

Fig. 4-2: Isolator configurations tested.

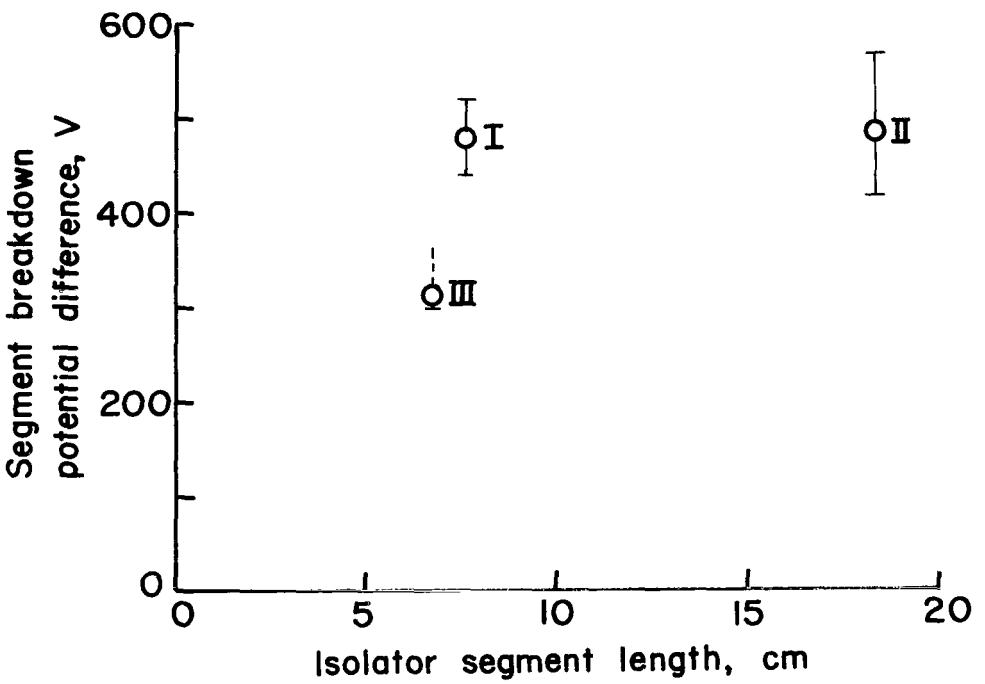

Fig. 4-3: Breakdown voltages per isolator segment, with thruster operating.

ranged from 630 to 1000 mA-equivalent for configuration I and from 600 to 1200 mA-equivalent for configuration II. Note that there was no significant difference in breakdown voltage for more than a factor of two increase in length. For configuration III, the voltage per segment was assumed to be one-third of the total voltage. This assumption gave a breakdown voltage per segment of about two-thirds of the values found for configurations I and II. This difference indicates that the voltage division between segments might be less even than assumed. The flows ranged from about 90 to 1000 mA-equivalent for configuration III. Several hours of operation were observed at 1000 V (333 V per segment) with no breakdowns at 600 mA-equivalent, or more. This absence of breakdown is indicated in Fig. 4-3 by the absence of an upper error bar for that configuration.

Observations were also made with similar propellant flows, but no thruster discharge. The breakdown potential differences under these conditions were several times as high as those shown in Fig. 4-3. From visual observations of the breakdowns, there was no doubt that the breakdowns were occurring inside of the isolator both with and without discharge. Apparently, then, some charged particles were able to traverse the stainless steel tube between the thruster and the isolator. This traversal is impressive inasmuch as the tubing was curved and had a total length-to-diameter ratio greater than 140:1. Because charged particles could reach the isolator from the thruster, an additional steel wool pad between the isolator and the thruster would be expected to improve the isolator performance.

V - CONCLUDING REMARKS

As mentioned in the Introduction, the advances in discharge-chamber technology obtained under this Grant have been included in an earlier publication.

Hollow cathode data were obtained for a wide range of operating conditions. No lifetime tests were conducted, but some neutralizer test conditions gave plasma coupling voltages at or below the sputtering threshold. Such conditions should permit long operating lifetimes.

All experimental observations of hollow cathodes were consistent with a single comprehensive theory of operation. That theory assumes a combination of thermionic and high field emission at localized areas within the orifice. This emission is assumed to exist at all conditions normally of interest in electric propulsion and supplements the emission from the insert. The emission from localized hot spots is supported by scanning electron microscope (SEM) photographs, which indicate localized melting has occurred at the tungsten tip near the orifice. In this theory, the difference between spot and plume modes is a function primarily of the neutral density at the exit of the orifice. In the spot mode, a high neutral density carries the ions into the plume region, effectively neutralizing the space charge of the electrons. In the plume mode, the low neutral density does not carry the ions in this manner. Instead, the ions are generated within the plume region, giving rise to the usual glow associated with this mode. With inert gases, though, the absence or presence of this glow was found to be a less definitive indicator of mode than with mercury.

Experimental hollow cathode performance with argon, krypton, and xenon propellants was correlated. Two orifice sizes were used with argon and

a range of flow rates was used with each of the three propellants. The parameters used in this performance correlation are consistent with the theory described above. For example, the emission parameter used is proportional to the square of the electric field in the orifice sheath. Also, the flow parameter that indicates the transition between spot and plume modes is proportional to the orifice diameter divided by mean free path. The degree of correlation obtained was excellent, considering the preliminary nature of the correlation study.

The basic theory for production of doubly ionized argon and xenon has been completed. Experimental measurements of the doubly ionized fraction agree with theory within about ±20 percent for the configurations and operating conditions tested. Both the neutral to doubly ionized and singly to doubly ionized processes are important in this theory. This result differs from that of mercury propellant, where the neutral to doubly ionized process was less important. Because both processes are important with argon and xenon, decreasing the discharge density will not be as helpful as with mercury in reducing the fraction of doubly ionized atoms.

For the isolator segment lengths investigated, the breakdown voltage per segment ranged from 300 to over 500 V. Multiple segment isolators should permit any reasonable total isolation voltage for electric propulsion to be sustained without breakdown. The difference between an operating discharge chamber and no discharge was a factor of several in isolator breakdown voltage, clearly indicating that some charged particles can traverse a feed tube with a length-to-diameter ratio of more than 140:1.

REFERENCES

SECTION I

1. Isaacson, G. C., "Multipole Gas Thruster Design," NASA Contractor Report CR-135101, June 1977.

SECTION II

1. Kaufman, H. R., "Inert Gas Thrusters," NASA Contractor Report CR-135100, July 1976.

2. Stuart, R. V., and Wehner, G. K., "Sputtering Yields at Very Low Bombarding Ion Energies," J. Applied Physics, Vol. 33, pp. 2345-2352, July 1962.

3. Askerov, Sh. G., and Sena, L. A., "Cathode Sputtering of Metals by Slow Mercury Ions," Soviet Physics - Solid State, Vol. 11, pp. 1288-1293, Dec. 1969.

4. Sovey, J. S., "Characteristics of a 30-cm Diameter Argon Ion Source," AIAA Paper No. 76-1017, Nov. 1976.

5. Isaacson, G. C., "Thick Sheath Langmuir Probe Analysis," Appendix B in NASA Contractor Report CR-134755, Dec. 1974.

6. Wilbur, P. J., "15 cm Mercury Ion Thruster Research - 1976," NASA Contractor Report CR-135116, Dec. 1976.

7. Kaufman, H. R., "Interaction of a Solar Array with an Ion Thruster due to the Charge-Echange Plasma," NASA Contractor Report CR-135099, Oct. 1976.

8. Rawlin, V. K., and Pawlik, E. V., "Mercury Plasma-Bridge Neutralizer," AIAA Paper No. 67-670, Sept. 1967.

9. Csiky, G. A., "Measurements of Some Properties of a Discharge from a Cathode," NASA Tech. Note TN D-4966, Feb. 1969. (A shorter version is given in J. Spacecr. Rockets, Vol. 7, pp. 474-475, Apr. 1970.)

10. Wilbur, P. J., Monthly Report on NASA Grant NGR-06-002-112, Aug. 5, 1977.

11. Cobine, J. D., Gaseous Conductors, pp. 246-247, Dover Publications, New York, 1958.

12. Wilbur, P. J., "15 cm Mercury Ion Thruster Research - 1975," NASA Contractor Report CR-134905, Dec. 1975.

13. Bessling, H., "Theorie de Hochtemperatur-Hohlkathode, ein Modell für den Kathodmechanismus," Deutsche Luft - und Raumfahrt, Forschungsbericht DLR-FB 76-50, 1976.

14. Anderson, G. S., "Hg Adsorption Studies Using Atom Ejection Patterns," J. App. Physics, Vol. 36, pp. 1558-1561, May 1965.

15. Newsome, D. S., "Significant Structure Theory of Multilayer Physical Adsorption," J. Physical Chemistry, Vol. 78, pp. 2600-2604, 1974.

16. Rehn, L. A., "Argon Hollow Cathode," NASA Contractor Report CR-135102 (Appendix), Nov. 1976.

17. Snyder, A., and Banks, B. A., "Thrust Measurements of a Hollow-Cathode Discharge," NASA Tech. Note TN D-6705, Mar. 1972.

18. Kaufman, H. R., "Technology of Electron-Bombardment Ion Thrusters," in Advances in Electronics and Electron Physics, Vol. 36. (L. Marton, ed.), pp. 265-373, Academic Press, New York, 1974.

SECTION III

1. Peters, R. R., "Double Ion Production in Mercury Thruster," NASA CR-135109, Apr. 1976.

2. Masek, T. D., "Plasma Properties and Performance of Mercury Ion Thrusters," AIAA Paper No. 69-256, March 3-5, 1969.

3. Kieffer, L. J., and G. H. Dunn, "Electron Impact Ionization Cross-section Data for Atoms, Atomic Ions, and Diatomic Molecules: I. Experimental Data," Rev. of Mod. Phys., Vol. 38, No. 1, pp. 1-35, Jan. 1966.

4. Isaacson, G., Private communication, Colorado State University, Feb. 1977.

DISTRIBUTION LIST

	No. of Copies
National Aeronautics and Space Administration Washington, D. C. 20546	
Attn: RPE/Mr. Wayne Hudson	1
Mr. Daniel H. Herman, Code SL	1
National Aeronautics and Space Administration Lewis Research Center 21000 Brookpark Road Cleveland, Ohio 44135	
Attn: Research Support Procurement Section	
Mr. Allen Jones, MS 500-313	1
Technology Utilization Office, MS 3-19	1
Report Control Office, MS 5-5	1
Library, MS 60-3	2
N. T. Musial, MS 600-113	1
Spacecraft Technology Division, MS 501-8	
Mr. H. Douglass	1
Mr. R. Finke	1
Mr. D. Byers	1
Mr. B. Banks	1
Mr. S. Domitz	1
Mr. F. Terdan	1
Mr. W. Kerslake	1
Mr. Vincent K. Rawlin	20
Mr. M. Mirtich	1
Physical Science Division, MS 301-1	
Mr. W. E. Moeckel	1
National Aeronautics and Space Administration Marshall Space Flight Center Huntsville, Alabama 35812	
Attn: Mr. Jerry P. Hethcoate	1
Research and Technology Division Wright-Patterson AFB, Ohio 45433	
Attn: (ADTN) Lt. David A. Fromme	1
NASA Scientific and Technical Information Facility P. O. Box 8757 Baltimore/Washington International Airport Baltimore, Maryland 21240	40
Case Western Reserve University 10900 Euclid Avenue Cleveland, Ohio 44106	
Attn: Dr. Eli Reshotko	1
Royal Aircraft Establishment Space Department Farnborough, Hants, England	
Attn: Dr. D. G. Fearn	1

United Kingdom Atomic Energy Authority
Culham Laboratory
Abingdom, Berkshire, England
Attn: Dr. P. J. Harbour 1
Dr. M. F. A. Harrison 1
Dr. T. S. Green 1

National Aeronautics and Space Administration
Goddard Space Flight Center
Greenbelt, Maryland 20771
Attn: Mr. W. Isley, Code 734 1
Mr. R. Bartlett, Code 713 1
Mr. R. Callens, Code 734 1

SAMSO
Air Force Unit Post Office
Los Angeles, California 90045
Attn: Capt. D. Egan/SYAX 1

Comsat Laboratories
P. O. Box 115
Clarksburg, Maryland 20734
Attn: Mr. B. Free 1
Mr. O. Revesz 1

Rocket Propulsion Laboratory
Edwards AFB, California 93523
Attn: LKDA/Mr. Tom Waddell 2

DFVLR - Institut für Plasmadynamik
Technische Universitat Stuttgart
7 Stuttgart-Vaihingen
Allmandstr 124
West Germany
Attn: Dr. G. Krülle 1
Mr. H. Bessling 1

Giessen University
1st Institute of Physics
Giessen, West Germany
Attn: Professor H. W. Loeb 1

Jet Propulsion Laboratory
4800 Oak Grove Drive
Pasadena, California 91102
Attn: Dr. Kenneth Atkins 1
Technical Library 1
Mr. Eugene Pawlik 1
Mr. James Graf 1

Electro-Optical Systems, Inc.
300 North Halstead
Pasadena, California 91107
Attn: Mr. R. Worlock 1
Mr. E. James 1
Mr. W. Ramsey 1

TRW, Inc.
TRW Systems
One Space Park
Redondo Beach, California 90278
Attn: Mr. M. Huberman 1
Dr. J. M. Sellen 1
Dr. S. Zafran 1

National Aeronautics and Space Administration
Ames Research Center
Moffett Field, California 94035
Attn: Technical Library 1

National Aeronautics and Space Administration
Langley Research Center
Langley Field Station
Hampton, Virginia 23365
Attn: Technical Library 1

Hughes Research Laboratories
3011 Malibu Canyon Road
Malibu, California 90265
Attn: Dr. Jay Hyman 1
Mr. J. H. Molitor 1
Dr. R. L. Poeschel 1
Mr. R. Vahrenkamp 1
Dr. John R. Beattie 1

United States Air Force
Office of Scientific Research
Washington, D. C. 20025
Attn: Mr. M. Slawsky 1

Princeton University
Princeton, New Jersey 08540
Attn: Mr. W. F. Von Jaskowsky 1
Dean R. G. Jahn 1
Dr. K. E. Clark 1

Communications Research Centre
Ottawa, Ontario, Canada
Attn: Dr. W. F. Payne 1

Joint Institute for Laboratory Astrophysics
University of Colorado
Boulder, Colorado 80302
Attn: Dr. Gordon H. Dunn 1

Department of Aeronautics and Astronautics
Stanford University
Stanford, California 94305
Attn: Professor Howard S. Seifert 1

Boeing Aerospace Company
P. O. Box 3999
Seattle, Washington 98124
Attn: Mr. Donald Grim 1

Intelcom Rad Tech
7650 Convoy Court
P. O. Box 80817
San Diego, California 92138
Attn: Dr. David Vroom 1

Lockheed Missiles and Space Company
Sunnyvale, California 94088
Attn: Dr. William L. Owens
Propulsion Systems, Dept. 62-13 1

Fairchild Republic Company
Farmingdale, New York 11735
Attn: Dr. William Guman 1

COMSAT Corporation
950 L'Enfant Plaza SW
Washington, D. C. 20024
Attn: Mr. Sidney O. Metzger 1

Electrotechnical Laboratory
Tahashi Branch
5-4-1 Mukodai-Machi, Tanashi-Shi
Tokyo, Japan
Attn: Dr. Katsuva Nakayama 1

Office of Assistant for Study Support
Kirtland Air Force Base
Albuquerque, New Mexico 87117
Attn: Dr. Calvin W. Thomas OAS Ge 1
Dr. Berhart Eber OAS Ge 1

Bell Laboratories
600 Mountain Avenue
Murray Hill, New Jersey 07974
Attn: Dr. Edward G. Spencer 1
Dr. Paul H. Schmidt 1

Massachusetts Institute of Technology
Lincoln Laboratory
P. O. Box 73
Lexington, Massachusetts 02173
Attn: Dr. H. I. Smith 1

Sandia Laboratories
Mail Code 5742
Albuquerque, N.M. 87115
Attn: Mr. Ralph R. Peters 1

Service du Confinement des Plasma
Centre d'Etudes Nucléaires - F.A.R.
B.P. 6
92260 Fontenay-aux-Roses
France
Attn: Dr. J. F. Bonal 1